Concentration and source changes of HONO during the COVID-19 lockdown in Beijing

Yusheng Zhang[1], Feixue Zheng[1], Zemin Feng[1,2], Chaofan Lian[3,4], Weigang Wang[3,4*], Xiaolong Fan[1,5,6], Wei Ma[1], Zhuohui Lin[1], Chang Li[1], Gen Zhang[7], Chao Yan[8,9], Ying Zhang[1,9],Veli-Matti Kerminen[1,8] , Federico Bianch[1,8], Tuukka Petäjä[1,8], Juha Kangasluoma[1,8], and Markku Kulmala[1,8], Yongchun Liu[1*]

1. Aerosol and Haze Laboratory, Advanced Innovation Center for Soft Matter Science and Engineering, Beijing University of Chemical Technology, Beijing, 100029, China

2. College of Chemical Engineering, North China University of Science and Technology, Tangshan 063210, China

3. State Key Laboratory for Structural Chemistry of Unstable and Stable Species, Beijing National Laboratory for Molecular Sciences (BNLMS), CAS Research/Education Center for Excellence in Molecular Sciences, Institute of Chemistry, Chinese Academy of Sciences, Beijing 100190, China

4. University of Chinese Academy of Sciences, Beijing 100049, China

5. Center for Excellence in Regional Atmospheric Environment, Institute of Urban Environment, Chinese Academy of Sciences, Xiamen 361021, China

6. Fujian Key Laboratory of Atmospheric Ozone Pollution Prevention, Institute of Urban Environment, Chinese Academy of Sciences, Xiamen 361021, China

7. State Key Laboratory of Severe Weather & Key Laboratory of Atmospheric Chemistry of China Meteorological Administration (CMA), Chinese Academy of Meteorological Sciences (CAMS), Beijing 100081, China

8. Institute for Atmospheric and Earth System Research/Physics, Faculty of Science, University of Helsinki, P.O. Box 64, FI-00014, Finland

9. Joint International Research Laboratory of Atmospheric and Earth System Science, School of Atmospheric Sciences, Nanjing University, Nanjing, China.

*Correspondence: Yongchun Liu (liuyc@buct.edu.cn) and Weigang Wang (wangwg@iccas.ac.cn)

Abstract:

Nitrous acid (HONO) is an important precursor of OH radicals which affects not only the sinks of primary air pollutants but also the formation of secondary air pollutants, whereas its source closure in the atmosphere is still controversial due to a lack of experiment validation. In this study, the HONO budget in Beijing has been analyzed and validated through the coronavirus disease (COVID-19) lockdown event, which resulted in a significant reduction in air pollutant emissions, providing a rare opportunity to understand the HONO budget in the atmosphere. We measured HONO and related pollutants from January 1, 2020, to March 6, 2020, which covered the Chinese New Year (CNY) and the COVID-19 lockdown. The average concentration of HONO decreased from 0.97 ± 0.74 ppb before CNY to 0.53 ± 0.44 ppb during the COVID-19 lockdown, accompanied by a sharp drop of NO_x and the greatest drop of NO (around 87%). HONO budget analysis suggests that vehicle emissions were the most important source of HONO during the nighttime ($53 \pm 17\%$) before CNY, well supported by the decline of their contribution to HONO during the COVID-19 lockdown. We found that the heterogeneous conversion of NO_2 on ground surfaces was an important nighttime source of HONO ($31 \pm 5\%$), while that on aerosol surfaces was a minor source ($2 \pm 1\%$). Nitrate photolysis became the most important daytime source during the COVID-19 lockdown compared with that before CNY, resulting from the combined effect of the increase in nitrate and the decrease in NO. Our results indicate that reducing vehicle emissions should be an effective measure for alleviating HONO in Beijing.

1. Introduction

As the most vital oxidant in the troposphere, OH radicals not only govern the sink of most trace compounds but also affect the production of secondary pollutants by initiating photochemical reactions in the atmosphere. Nitrous acid (HONO) is an important primary precursor of OH radicals (Kulmala and Petäjä, 2011; Zhang et al., 2023c). Photolysis of HONO can contribute 60% (Tan et al., 2018) and sometimes even 92% (Xue et al., 2020) to OH production in the morning. Therefore, HONO can indirectly promote the formation of both secondary aerosols (Zhang et al., 2019b) and ozone (Zhang et al., 2022a). In addition, HONO can react with histamine to form carcinogens, such as nitrosamines, after entering the human body (Farren et al., 2015). Thus, understanding the sources of HONO in the atmosphere has been a hot topic for several decades, but it is still far from closed (Jiang et al., 2022). Intensive studies have been carried out on HONO measurements and source analysis (Liu et al., 2020c; Liu et al., 2020d; Zheng et al., 2020; Zhang et al., 2020; Xue et al., 2020; Zhang et al., 2019a; Liu et al., 2019b). The concentrations of HONO in the atmosphere range from a few ppt in remote areas (Spataro et al., 2016) to several ppb, even several tens ppb in heavily polluted areas (Liu et al., 2019b; Liu et al., 2020c; Liu et al., 2020d; Zheng et al., 2020).

The sources of atmospheric HONO consist of direct emissions and secondary formation in the atmosphere. Direct emissions include soils, biomass burning, vehicles, indoor air, and livestock farming. Soil emissions, which depend on soil types, microorganisms, water content, temperature, and pH (Kulmala and Petäjä, 2011; Weber et al., 2015; Kim and Or, 2019), are important sources of HONO. Biomass burning, often occurs in the summer and autumn when wheat/corn is harvested and wildfires are common (Zhang et al., 2019b; Sun et al., 2017; Sun

73 et al., 2018; Peng et al., 2020). Vehicle emissions are considered an important source of HONO

74 in traffic-intensive areas (Kramer et al., 2020; Li et al., 2021). This source is more important at

75 nighttime compared with daytime (Zhang et al., 2016; Fu et al., 2019; Liu et al., 2020d).

76 Recently, indoor emissions have also been proposed as a potential HONO source (Xue, 2022),

77 which is related to the ventilation from high HONO concentrations in indoor air to low HONO

78 concentrations in outdoor air (Zhang et al., 2019b). Livestock farming is a previously

79 overlooked source of HONO, especially in agricultural areas.

80   Secondary formation of HONO includes gas-phase reaction between NO and OH radicals,

81 photolysis of particulate nitrate, and heterogeneous reaction of NO_2 on ground and particulate

82 matter surfaces, including photochemical heterogeneous reaction of NO_2. Gas phase reaction

83 between NO and OH, photolysis of nitrate particles, and light-enhanced conversion of NO_2 are

84 the main daytime sources of HONO (Liu et al., 2019c; Liu et al., 2020d; Zhang et al., 2022b).

85 Furthermore, acid replacement processes may be a non-negligible source of daytime HONO in

86 locations affected by soil-borne mineral dust deposition (Vandenboer et al., 2014). The

87 heterogeneous reaction of NO_2 on various surfaces is widely regarded as an important source

88 of HONO (Han et al., 2016; Liu et al., 2020b).

89   Table S1 summarizes the sources of HONO at various locations. The type of observation

90 site often has a great impact on the source intensity and contribution proportion of each source

91 of HONO. In natural ecological areas or Antarctic stations with little human activity, the

92 photolysis of nitrate is the main source of HONO during the day, and its contribution is much

93 higher than the homogeneous reaction of NO and OH (Bond et al., 2023; Tang et al., 2024). In

94 the ocean or areas close to the sea, the heterogeneous transformation of NO_2 becomes the main

source of HONO, and the transformation on the aerosol surface may be more important than that on the ground (Xing et al., 2023). In smoke collected near wildfires, it was found that the heterogeneous conversion contribution of NO_2 can reach 85%, making it the most important source of HONO (Chai et al., 2021). Emissions from soil and biological soil crusts are important in some areas where vegetation and soil are exposed (Meusel et al., 2018). For three different types of observation sites: rural, suburban, and urban, the relative importance of sources is also obviously different. In rural areas, there are usually no traffic activities, and are mainly affected by agricultural activities and animal husbandry, so traffic emissions can be ignored. During periods of intensive agricultural activity, soil emissions are the main source of HONO, accounting for up to 80% (Liu et al., 2019c), When there is little agricultural activity, the reaction of NO and OH and the heterogeneous transformation of NO_2 on the ground become the two main sources in rural areas (Xue et al., 2020; Song et al., 2022), accounting for up to 70%. In rural areas with developed animal husbandry, its direct emissions can contribute 39-45% of HONO (Zhang et al., 2023a). Suburbs are mostly covered by vegetation, with a small number of villages nearby. The heterogeneous conversion of NO_2 is the main source of HONO, which can reach 70% of HONO sources (Fu et al., 2019; Ye et al., 2023). For highways, tunnels, and urban areas with heavy traffic, traffic emissions usually dominate HONO sources, accounting for 40% to 80% of HONO sources (Xu et al., 2015; Zhang et al., 2019c; Liu et al., 2020d; Kramer et al., 2020). In some ordinary urban areas where traffic activities are not so intensive, the heterogeneous conversion of NO_2 and the reaction of NO and OH are also the main sources of HONO in addition to traffic sources. It can be seen that the relative importance of different sources is often affected by the type of emission source near the observation site.

Although intensive studies have been performed on HONO sources, the contributions of different sources are still controversial (Zhou et al., 2011; Liu et al., 2014; Wu et al., 2019; Kramer et al., 2020; Meng et al., 2020). For the same type of observation area, the contribution of each source still diverges in different studies. For example, in mixed residential, commercial, and traffic areas, the importance of traffic emissions varies greatly. In some studies, it accounts for as much as 50% (Liu et al., 2020d; Zhang et al., 2019a; Tong et al., 2016), while in some studies, it can be ignored (Zhang et al., 2020). A similar situation exists for the heterogeneous conversion of NO_2. Some studies suggest that this process is not important (Tong et al., 2015; Zhang et al., 2019c; Zhang et al., 2022b), while some studies believe that it can contribute at least 70% of HONO (Meng et al., 2020; Zhang et al., 2020; Jia et al., 2020). It should be noted that the contribution of NO_2 heterogeneous reaction to HONO greatly depends on the choice of NO_2 uptake coefficient (γ_{NO2}), which varies from 10^{-8} to 10^{-4} in different studies (Meng et al., 2020; Liu et al., 2020b; Ge et al., 2019; Liu et al., 2015; Liu et al., 2020d). Vehicle emissions also have similar characteristics because the HONO emission rate strongly depends on the emission factor, i.e. the ratio of $HONO/NO_x$ (Kramer et al., 2020; R. Kurtenbach et al., 2001; Zhang et al., 2019c), which ranges from 0.03% to 2.1% (Liao et al., 2021). For other HONO sources, the relative importance is affected by many parameters, such as reaction kinetics for photolysis of nitrate, OH concentrations for homogeneous reaction between NO and OH, emission fluxes for soil emissions, and so on. Thus, the HONO budget still has a large uncertainty. In particular, it is an open question how to prove the importance of a specific reaction pathway or a source of atmospheric HONO.

Special events taking place on large spatial scales provide us with an alternative

139 opportunity to disclose the mysteries of the HONO budget because of obvious and potentially

140 large changes in some of the HONO sources. During the Spring Festival in 2020, the lockdown

141 measures during the new coronavirus disease -19 (COVID-19) pandemic led to a significant

142 reduction in primary emissions from traffic and industries. The magnitude and speed of changes

143 in air pollutant emissions have been considered the largest changes in the history of modern

144 atmospheric chemistry (Kroll et al., 2020). We conducted continuous field observations of

145 HONO and other air pollutants from January 1, 2020, to March 6, 2020, in downtown Beijing,

146 aimed at understanding the changes in HONO concentrations and sources during the lockdown

147 period compared to that before.

148 **2. Experimental section**

149 **2.1 Field measurements.**

150 Observations were carried out at the Aerosol and Haze Laboratory, Beijing University of

151 Chemical Technology (AHL/BUCT), which has been described in our previous work (Liu et

152 al., 2020d). Briefly, it is located on the west campus of BUCT, around 550 m from the west

153 third-ring road of Beijing, which is a typical urban observation site. The station is on the rooftop

154 of a 5-story building (about 18 m from the ground). HONO was measured with a homemade

155 Water-based Long-Path Absorption Photometer (LOPAP, Institute of Chemistry, Chinese

156 Academy of Sciences), which has been deployed in field observation studies (Tong et al., 2016;

157 Chen et al., 2020) and has been proven to be a stable and credible instrument for HONO

158 measurements (Crilley et al., 2019). The principle of this instrument is similar to that of a

159 commercial LOPAP (QUMA). Briefly, gas-phase HONO absorbed by deionized water ($\geq$ 18.2

160 MΩ) in a stripping coil reacts with N-(1-naphthyl) ethylenediamine-dihydrochloric acid (0.077

161   mmol L^{-1}) in an acidic solution (2 mmol L^{-1} sulfanilamide in 0.12 mol L^{-1} HCl) to form an azo

162   dye, which is measured at 550 nm with a spectrometer equipped with a LWCC (Liquid

163   Waveguide Capillary Cell, LWCC-3250, WPI, USA). The sampling rate was 1 L min^{-1}

164   controlled by a flow meter and a diaphragm pump. The flow rate of absorption liquid was 0.5

165   ml min^{-1} controlled by a peristaltic pump. The limit of detection of the LOPAP was 0.01 ppb

166   for a sampling duration of 60 s. The instrument was calibrated with nitrite standard solution

167   before and after each measurement about every three weeks and calibrated by zero air every

168   24 hours to check zero drift. An overestimation of HONO concentration (6.7%), calibrated in

169   control experiments with 100 ppb of NO_2 at 50% RH due to the interference of NO_2 in the

170   sampling inlet (about 30 cm of Teflon tube), was accounted for when we calculating the HONO

171   concentrations in this work.

172   A set of commercial analyzers for NO_x, SO_2, CO, and O_3 (Thermo Scientific 42i, 43i, 48i,

173   49i) were also available. Notably, the NO_2 measured by 42i includes HONO, and we have

174   corrected it. $PM_{2.5}$ was measured using a Tapered Element Oscillating Microbalance (TEOM,

175   Thermo Fisher Scientific, 1405). The chemical composition of non-refractory $PM_{2.5}$ (NR-$PM_{2.5}$)

176   was measured using a Time-of-flight Aerosol Chemical Speciation Monitor (ToF-ACSM,

177   Aerodyne). Meteorological parameters including temperature, RH, pressure, wind speed and

178   direction, and ultraviolet radiation (A and B) were measured using a weather station (AWS 310

179   at AHL/BUCT station, Vaisala). The planetary boundary layer (PBL) height and visibility were

180   measured using a ceilometer (CL51, Vaisala) and a visibility sensor (PWD22, Vaisala),

181   respectively. The photolysis rate (J_{NO2}) was measured via a continuous measurement of the

182   actinic flux in the wavelength range of 285-375 nm using a J_{NO2} filter-radiometer (2-pi-J_{NO2}

183   radiometer, Metcon). All instruments used in the measurement as well as their detection limits

184   are shown in Table S2.

2.2 HONO budget calculation.

186   Potential sources of HONO include direct emissions (vehicle emissions, soil emissions, indoor

187   emissions, biomass combustion), the gas-phase reaction between NO and OH radicals, the

188   photolysis of nitrate in particulate matter, and the heterogeneous reaction of NO_2 on the ground

189   and particulate matter surfaces. The sources including vehicle emissions ($E_{vehicle}$), soil

190   emissions (E_{soil}), the reaction of NO and OH (P_{NO-OH}), the photolysis of particulate nitrate

191   ($P_{nitrate}$), and the heterogeneous reaction of NO_2 ($P_{aerosol}$ and P_{ground}). At present, there are

192   relatively few studies on indoor emissions. Biomass combustion is an unimportant HONO

193   source in downtown Beijing in winter according to a previous study (Zhang et al., 2019b). Thus,

194   these two sources are not accounted for in this work. The major sinks of HONO, including dry

195   deposition ($L_{deposition}$), the homogeneous reaction with OH radicals ($L_{HONO-OH}$), photolysis

196   ($L_{photolysis}$), and vertical and horizontal transport (T_{trans}), are considered.

197   The calculation method and details in parameterization are shown in Table 1. Briefly, the

198   budget and estimated concentration of HONO can be calculated according to the following

199   equations,

$$\frac{dHONO}{dt} = E_{soil} + E_{vehicle} + P_{NO-OH} + P_{nitrate} + P_{aerosol} + P_{ground} -$$

$$L_{photolysis} - L_{HONO-OH} - L_{deposition} - T_{trans} \tag{1}$$

$$HONO_{est,t_2} = HONO_{obs,t_1} + Sources_{t_2} - Sinks_{t_2} \tag{2}$$

203   where $\frac{dHONO}{dt}$ is the change rate of HONO mixing ratios (ppb h^{-1}), $HONO_{est,t_2}$ is the

204   estimated concentration of HONO at time t$_2$, while $HONO_{obs,t_1}$ is the observed concentration

205 of HONO at time t_1. Given that the result of potential source contribution function (PSCF, Fig

206 S2), the source distribution of HONO between BCNY and COVID was highly similar and the

207 trend of HONO was similar (Pearson'r=0.78) between BUCT and Institute of Atmospheric

208 Physics (IAP, 8 km away from BUCT), the steady state analysis on HONO is appliable and

209 reasonable even though the lifetime of HONO is several minutes in the atmosphere. In addition,

210 the instrumentation time resolution of LOPAP was 6 s. We calculated the variation coefficient

211 for the datasets with different time resolutions, i.e., 1 h *vs* 6 s. A small variation coefficient of

212 ~0.02-0.05 implies that a small uncertainty of the HONO budget might result from the lifetime

213 of HONO. Thus, we think the possible uncertainty should not have a large influence on our

214 conclusions when the budget is compared at a fixed site between two different periods. The

215 input parameters for the parameterization scheme are detailed in Table S3 (M0).

216   The emission rate (E_{HONO}, ppb h^{-1}) of soil and vehicle were calculated based on the

217 emission flux (F_{HONO}, g m^{-2} s^{-1}), the PBL height (H, m), and the conversion factor (α, g m^{-3} s^{-1}

218 to ppb h^{-1}). For vehicle emissions, according to our previous research at the same site, the

219 emission factor (EF, HONO/NO$_x$) was selected as 1.09% (Liu et al., 2020d), which is

220 comparable to the actual values in Hong Kong (1.2 ± 0.4% and 1.24 ± 0.35%) (Liang et al.,

221 2017; Xu et al., 2015), Guangzhou (1.0%) (Li et al., 2012), Beijing (1.3% and 1.41%) (Zhang

222 et al., 2019c; Meng et al., 2020), and other places. For secondary formation, the calculation of

223 the production rate (P_{HONO}, ppb h^{-1}) is shown in Table 1, in which k_1 is the rate constant of the

224 quasi-first order reaction (s^{-1}). For the heterogeneous reaction of NO$_2$, we calculated the

225 conversion rate in the light of Eqs. (3)-(5):

226 $$k_{het}^0 = \frac{HONOcorr,t_2 - HONOcorr,t_1}{\overline{NO_2} \times (t_2 - t_1)} \qquad (3)$$

$$227 \quad k_{het}^{co} = \frac{2\times\left[\frac{HONOcorr,t_2}{CO_{t_2}}\times\overline{CO} - \frac{HONOcorr,t_1}{CO_{t_1}}\times\overline{CO}\right]}{(t_2-t_1)\times\left[\frac{NO_{2,t_2}}{CO_{t_2}}+\frac{NO_{2,t_1}}{CO_{t_1}}\right]\times\overline{CO}}$$

$$228 \qquad\qquad = \frac{2\times\left[\frac{HONOcorr,t_2}{CO_{t_2}} - \frac{HONOcorr,t_1}{CO_{t_1}}\right]}{(t_2-t_1)\times\left[\frac{NO_{2,t_2}}{CO_{t_2}}+\frac{NO_{2,t_1}}{CO_{t_1}}\right]} \qquad (4)$$

$$229 \qquad k_{het} = \frac{1}{2}\times(k_{het}^0 + k_{het}^{co}) \qquad (5)$$

230   where k_{het} is the quasi-first-order rate constant of the transformation to HONO (s⁻¹), k_{het}^0

231   and k_{het}^{co} are the reaction rate constants after uncalibrated and CO calibrated, respectively

232   (Zhang et al., 2020). To decrease the contribution of boundary layer height variation on the k_{het}

233   calculations, we normalized HONO concentration to CO concentration as the same as reported

234   in the literature (Zhang et al., 2019c; Li et al., 2012). $\overline{NO_2}$ and $\overline{CO}$ are the mean

235   concentration of NO_2 and CO from t_1 to t_2. CO_t and $NO_{2,t}$ are mixing ratios of CO and NO_2,

236   respectively, at the measuring time t. HONO$_{corr,t}$ (ppb) is the HONO concentration corrected

237   after subtracting the primary emissions (including vehicle and soil emissions, and the HONO

238   produced by the homogeneous reaction of NO and OH and the photolysis of nitrate) at the

239   measuring time t according to Eq. (6):

$$240 \qquad HONO_{corr,t} = HONO_t - E_{soil,t} - E_{vehicle,t} - P_{NO-OH,t} - P_{nitrate,t} \qquad (6)$$

241   it is worth noting that the $HONOcorr$ only accounted for vehicle exhausts in previous HONO

242   budget studies. This may overestimate the contribution of heterogeneous reactions to HONO

243   sources because other emission sources and homogeneous reactions should also contribute to

244   HONO.

245   Meanwhile, when estimating the upper limit of the contribution of heterogeneous

246   reactions, we take a small conversion factor (HONO/NOx) of 0.4% as the lower limit of vehicle

247   emissions, in contrast to the normal value of 1.09% (Liu et al., 2020d). We normalize the

248 EI_{NO_X} caused by the vehicle with the measured NO_X during the observations. This method

249 has also been widely used in previous studies (Liu et al., 2019b; Li et al., 2018). In addition,

250 soil emissions are calculated using the lower limit (Oswald et al., 2013). The mean value of

251 k_{het} during the BCNY (before the Chinese New Year) was 0.0051 h^{-1}, while it was 0.006 h^{-1}

252 in the COVID-19 lockdown, which are consistent with previous studies, such as Ji'nan (0.0068

253 h^{-1}) (Li et al., 2018) and Shanghai (0.007 h^{-1}) (Wang et al., 2013), while less than those in

254 Shijiazhuang (0.016 h^{-1}) (Liu et al., 2020c), Kathmandu (0.014 h^{-1}) (Yu et al., 2009), and

255 Guangzhou (0.016 h^{-1}) (Qin et al., 2009).

Table 1. Summary of parameters for HONO sources and sinks

HONO formation/loss pathways	Calculations	Parameters	Reference
Soil emissions → HONO		$F_{HONO,soil}$	1
Vehicle emissions → HONO	$E_{HONO} = \alpha \times F_{HONO}/H$	$F_{HONO,vehicle} = (EI_{NOx,vehicle}/A) \times (HONO/NOx)_{vehicle}$	2
NO + OH → HONO		$k_{NO\text{-}OH} = 7.2 \times 10^{-12}\,cm^3\,molecule^{-1}\,s^{-1}$	3
$NO_3^- \xrightarrow{hv} HONO$		$J_{NO3^-} = 8.24 \times 10^{-5}/3.59 \times 10^{-7} \times J_{HNO3,MCM}$	
$NO_2 + H_2O \xrightarrow{aerosol\ surface} HONO$	$P_{HONO} = 3600 \times k \times c_{precursor}$	$k_{het} = (\gamma_{NO2} \times A_s \times \omega/4) \times Y_{HONO}$	4
$NO_2 + H_2O \xrightarrow{ground\ surface} HONO$		$k_{het} = (\gamma_{NO2} \times \delta \times \omega/4H) \times Y_{HONO}$	
$HONO \xrightarrow{hv} NO + OH$	$L_{photolysis} = 3600 \times J_{HONO} \times HONO$	$J_{HONO,\ MCM}$	
HONO + OH → H_2O + NO_2	$L_{HONO\text{-}OH} = 3600 \times k_{HONO\text{-}OH} \times HONO \times OH$	$k_{HONO\text{-}OH} = 6 \times 10^{-12}\,cm^3\,molecule^{-1}\,s^{-1}$	5
HONO deposition	$L_{deposition} = (3600 \times V_d \times HONO)/H$	$V_d = 0.001\,m\,s^{-1}$	6
HONO transport (vertical and horizontal)	$T_{trans} = k_{dilution} \times (HONO\text{-}HONO_{background})$	$k_{dilution} = 0.23\,h^{-1}$	7

$F_{HONO,soil}$ (soil emission flux) was calculated by the temperature-dependent HONO emission flux on grasslands with a water content of 35% to 45%. A is the urban area of Beijing, $EI_{NOx,vehicle}$ is the emission inventory of NO_x from vehicle (g s^{-1}). The calculation of the HONO emission flux, during BCNY, was based on the hourly NO_x emission inventory of Beijing vehicles ($F_{HONO}=F_{NOx} \times (HONO/NOx)_{vehicle}$), while during COVID-19, it was combined with the hourly average traffic index (www.nitrafficindex.com). The $(HONO/NOx)_{vehicle}$ was selected as 1.09% (Liu et al., 2020d). $c_{precursor}$ is the concentration of the precursor (ppb). The OH concentration was estimated using the same method as in the previous study (Liu et al., 2020c). The mean photolysis frequency of nitrate (J_{NO3^-}) was normalized to the measured UV light intensity. A_s is the surface area concentration of the reaction surface (m^2 m^{-3}); ω is the average molecular velocity (m s^{-1}); γ is the uptake coefficient of the precursor, was assumed to be 2×10^{-6}; Y_{HONO} is the yield of HONO. δ is the surface roughness, in this study, we used 3.85 for our calculation (Liu et al., 2020d). $HONO$ and $HONO_{background}$ are the HONO concentrations at the observation site and background site, respectively. J_{HONO} is simulated in a box model using J_{NO2} data observed at our site.

1: (Oswald et al., 2013). 2: (Yang et al., 2019). 3: (Liu et al., 2020c). 4: (Liu et al., 2020d). 5: (Kanaya et al., 2007). 6: (Han et al., 2017b). 7: (Dillon et al., 2002).

257

258   We further derived the uptake coefficient of NO₂ (γ_{NO2}) on both ground and particle

259   surfaces according to Eq. (7).

260     $$k_{het} = \frac{\gamma_{NO2} \times A_s \times \omega}{4} \times Y_{HONO} \qquad (7)$$

261   The calculated γ_{NO2} ranged from 1×10^{-6} to 3×10^{-6}. Therefore, we choose

262   2×10^{-6} to calculate the heterogeneous yield of HONO, which is comparable with those

263   derived in urban environments like Ji'nan (1.4×10^{-6}) (Li et al., 2018) and the laboratory

264   experiments (10^{-7} to 10^{-6}) (Han et al., 2013; Stemmler, 2007; Han et al., 2017a) on different

265   particles, but lower than the uptake coefficient of 10^{-5} reported in other studies (Zhang et al.,

266   2020; Ge et al., 2019).

267   The OH concentration was calculated according to Eq. (8), which is based on the function

268   of the photolysis rates (*J*) of O₃ and NO₂, and the NO₂ mixing ratio (*NO₂*).

269     $$OH = \frac{4.1 \times 10^9 \times (J_{NO2})^{0.19} \times (J_{O1D})^{0.83} \times (140 NO_2 + 1)}{0.41 NO_2^2 + 1.7 NO_2 + 1} \qquad (8)$$

270   Notably, this parameterization scheme was developed based on measurements at rural sites

271   (Ehhalt and Rohrer, 2000), where NOx concentrations were lower than in urban environments.

272   Alicke et al. (Alicke, 2002) found that OH concentrations estimated with this scheme were in

273   good agreement with those calculated according to a pseudo-steady state method during the

274   pollution period in urban environments (such as Milan), although some uncertainty was

275   expected. In our previous study (Liu et al., 2020d), we also found that the estimated OH

276   concentrations using this method were comparable with those observed values in the North

277   China Plain (Tan et al., 2019). Thus, daytime OH concentrations estimated using this method

278   should be overall credible although the uncertainty is inevitable. The nocturnal OH

279   concentration in North China generally varied from 1.0×10^5 molecules cm^{-3} (Ma et al., 2019;

280 Tan et al., 2018) in winter to 5×10^5 molecules cm^{-3} in summer (Tan et al., 2017; Tan et al.,

281 2020). We further parameterized the nocturnal OH concentrations according to atmospheric

282 temperature to reflect the seasonal variations of OH concentration. Fig. S3 summarizes the

283 observed OH concentrations in the North China Plain. The results estimated in this study are

284 slightly lower than those observed in Wangdu (Rural), but almost consistent with those in

285 Beijing (Urban) and Huairou (Suburb). In summary, we should be optimistic about the

286 estimation of OH concentration. Then a sensitivity analysis was performed to understand the

287 influence of the uncertainty of OH concentration on HONO sources as discussed in Section 3.3.

288   The loss rate of HONO, including dry deposition ($L_{deposition}$), homogeneous reaction

289 with OH radicals ($L_{HONO-OH}$), photolysis ($L_{photolysis}$), and vertical and horizontal transport

290 (T_{trans}), were calculated using the equations shown in Table 1. Where J_{HONO} is the photolysis

291 rate of HONO (s^{-1}), $k_{HONO-OH}$ is the second-order reaction rate constant between HONO and

292 OH, V_d is the dry deposition rate of HONO, and $K_{dilution}$ is the dilution rate (including both

293 vertical and horizontal transport). The details are described in our previous work (Liu et al.,

294 2020c; Liu et al., 2020d).

295   Oracle Crystal Ball (version 11.1.2.4, Oracle's software for modeling, prediction,

296 simulation, and optimization) (Rahmani et al., 2023) to evaluate the overall uncertainty of the

297 parameterization through Monte Carlo simulations. The details are shown in Text S2 in the SI.

298 **3. Results and discussion**

299 **3.1 Air quality during observations.**

300 Figure 1 shows the time series of the concentration and relative proportion of non-refractory

301 components in PM$_{2.5}$, trace gases (SO$_2$, O$_3$, CO, NO, NO$_2$, and NO$_x$), and meteorological

parameters (temperature, relative humidity (RH), and pressure). We divide the sampling period

into two sub-periods, i.e., P1 from January 1 to January 24 (BCNY, before the Chinese New

Year) and P2 from January 25 to March 6 (COVID-19 lockdown).
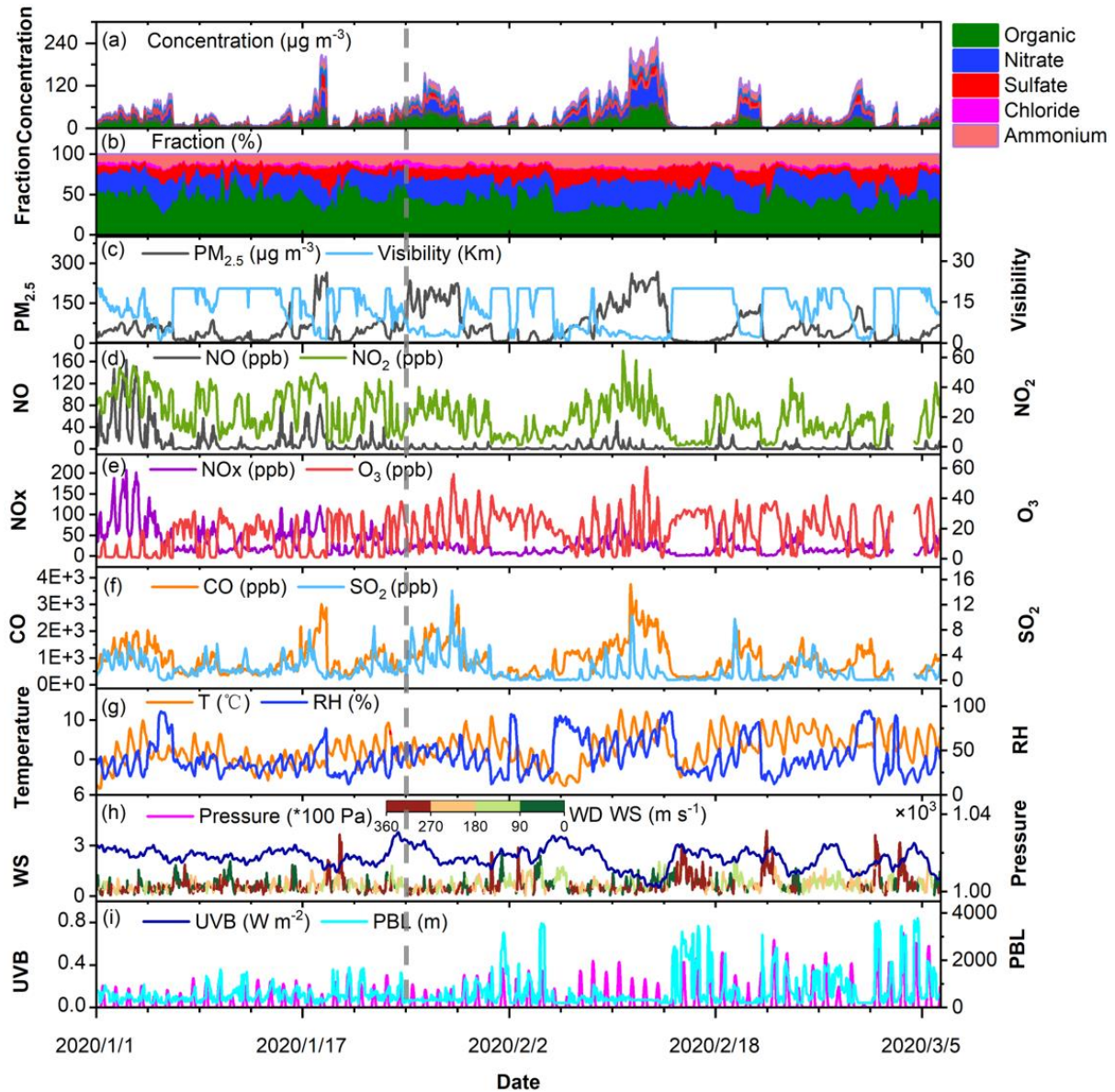
Figure 1. An overview of the measurement of the mass concentrations of the different

components of non-refractory-PM2.5 (NR-PM2.5), the mass fraction of the individual

components, PM2.5, and meteorological parameters, NO_x (NO, NO2), O3, CO and SO2 in 1-hour

average from 1 January to 6 March 2020. Meteorological parameters consist of visibility, PBL

heights, UVB, wind speed, wind direction, Pressure, RH, and temperature. The observations

311   are divided into two phases (P1:2020.01.01-2020.01.24 and P2:2020.01.25-2020.03.06).

312

313   It can be seen from Fig. 1 that during P1, there was only one heavy pollution incident

314   lasting one to two days, while there were two serious pollution events lasting more than two

315   days ($PM_{2.5} > 75$ µg m^{-3}) in the P2 stage. Table S4 summarizes the statistical results of the wind

316   speed, $PM_{2.5}$, RH, T, HONO, trace gases, and NR-$PM_{2.5}$ for the entire measurement period.

317   During P1, the measured concentration of $PM_{2.5}$ varied between 0.2-288 µg m^{-3} and the mean

318   concentration was 47.2 ± 44.5 (mean ± 1σ) µg m^{-3}. In contrast, they were 0.3-258 µg m^{-3} and

319   69.9 ± 67.2 µg m^{-3}, respectively, during P2. The mean concentrations of NO_x decreased

320   significantly (P < 0.05) from 45.35 ± 38.86 ppb in P1 to 19.44 ± 14.42 ppb in P2, dropping by

321   about 57%. This is close to the reduction amplitude (50%) reported by Wang et al. (Wang et

322   al., 2020a) but lower than that (76%) proposed by Lv et al (Lv et al., 2020). In particular, the

323   NO mean concentrations dropped from 18.42 ± 29.24 ppb (ranging from 0.03 to 163 ppb) in

324   P1 to 2.4 ± 5.46 ppb (ranging from 0.01 to 51 ppb). The average hourly concentration of NO_2

325   in the P1 phase was 26.9 ± 13.4 ppb, while it was 17.18 ± 11.3 ppb in P2. The NO_2

326   concentration dropped by about 36% from P1 to P2, which is similar to the recently reported

327   findings (ranging from 36% to 53%) (Zhao et al., 2020; Wang et al., 2020b; Wang et al., 2021).

328   According to the emission inventory of NO_x, traffic and industry contributed 46.7% and 31.3%

329   to NO_x emissions in Beijing, respectively (Zheng et al., 2014). This means the decrease in NO_x

330   concentration should be explained by both reductions in traffic and industrial emissions (Lv et

331   al., 2020; Wang et al., 2020a; Zhao et al., 2020). In particular, traffic emissions during P2

332   should play an important role in local NO reduction. However, as the temperature and

333 ultraviolet light irradiation increased and the NO_x concentration decreased (Kroll et al., 2020;

334 Le et al., 2020), the average concentration of O_3 during P2 was 21.31 ± 11.73 ppb, which was

335 significantly ($P < 0.05$) higher than 12.16 ± 10.79 ppb during P1. This result is similar to the

336 71.4% increase in O_3 in Shijiazhuang during the same period (Liu et al., 2020c). The

337 concentrations of SO_2 were in the range of 0.02-8.56 ppb with a mean value of 2.09 ± 1.35 ppb

338 in P1, while it varied from 0.01 to 14.23 ppb with the mean concentration of 1.49 ± 1.99 ppb

339 during P2, suggesting slightly decreased contribution of coal combustion during P2 (Fig. 1i).

340 This is similar to that reported by Cui et al (Cui et al., 2020) and Shen et al (Shen et al., 2021).

341 In addition, it can be seen from Fig. 1 that the change trends of $PM_{2.5}$ and CO are synchronized,

342 which also means that both primary emissions and secondary generation contribute to the

343 accumulation of $PM_{2.5}$ concentration (Liu et al., 2020c).

344   It is worth noting that changes in atmospheric pollutant concentrations are affected by

345 both emissions and meteorology. Especially, during the lockdown period, meteorological

346 conditions in Beijing were not conducive to the dispersion of pollutants, thus the impact of

347 meteorological conditions on the concentration of these pollutants needs to be assessed. We

348 use the random forest algorithm of machine learning to remove the influence of meteorology

349 from air quality time series data by a deweather method. The details are present in Text S1 in

350 the SI. The model performs well in predicting the concentrations of pollutants compared to the

351 observations in both the training and test datasets (Table S5). The concentrations and relative

352 changes of each pollutant after deweather are recorded in Table S6. The $PM_{2.5}$ concentration

353 after deweather increased significantly from 45.22 ± 28.56 in P1 to 67.92 ± 57.97 $\mu g\ m^{-3}$ in P2 at

354 a confidence level of 0.05, with an increase of 50.2%. The mean concentration of HONO was

355 0.89±0.37 ppb in P1, while it decreased to 0.51±0.25 ppb in P2, with a drop of 42.7%; The

356 concentrations of NO and NO_2 significantly decreased from 15.44±18.40 and 23.28±7.28 ppb

357 in P1 to 3.24±2.05 and 16.43±5.98 ppb in P2, respectively, which decreased by 79.0% and 29.4%

358 respectively; SO_2 decreased from 2.27±0.69 in P1 to 1.48±1.18 ppb in P2, a decrease of

359 approximately 34.8%; CO increased from 823.60±318.92 in P1 to 896±488.29 ppb in P2 (an

360 increase of 8.79%) and O_3 increased from 16.98±5.62 to 22.60±4.10 ppb, an increase of about

361 33.1%, which was much lower than the change range of observed values (75.1%). As shown

362 in Table S6, meteorological conditions have a significant impact on O_3 concentration. The

363 impact was +39.6% and +6.2% in P1 and P2, respectively. The impact of deweather on NO in

364 the two periods was -16.2% and +32.8%, respectively. It was -13.8% and -4.8%, respectively,

365 for NO_2. However, the changes of other species in the two periods after deweather fluctuated

366 between 2.3% and 7.8%. This implies that meteorological conditions have an important impact

367 on the concentrations of NO and O_3, while meteorological factors have little impact on HONO,

368 SO_2, CO, and $PM_{2.5}$.

369   It can be seen from Figure 1 combined with Table S4 in SI. All the major components of

370 $PM_{2.5}$, including sulfate, nitrate, ammonium, chloride, and organic aerosol, increased obviously

371 in P2 compared to P1. Throughout the entire observation period, organic matter and nitrate

372 dominated the composition of $PM_{2.5}$. The proportion of nitrate in inorganic salts increased to

373 31.2% in P2, up from 28.1% in P1. Although the sulfate concentration increased, its proportion

374 within inorganic salts slightly decreased on haze days, going from 16.5% in P1 to 15.2% in P2.

375 Thus, the ratio of NO_3^- to SO_4^{2-} during pollution events increased significantly from 1.76 in P1

376 to 2.10 in P2 (P < 0.05). This is similar to previous findings reported by Sun (Sun et al., 2020).

377 These findings suggest that the decrease in anthropogenic emissions during the P2 period

378 resulted in a significant reduction (After the T-test, it is significant at a confidence level of 0.01.)

379 in gas precursors (Table S4), but it did not lead to a corresponding reduction in secondary

380 aerosol species during periods of pollution. This is supported by the increased potential

381 secondary aerosol formation under pollution conditions (Sun et al., 2020). For example, higher

382 values of the SOR (sulfur oxidation ratio, molar fraction of sulfate in total sulfur including

383 sulfate and SO_2) and NOR (nitrogen oxidation ratio, molar fraction of nitrate in total nitrogen,

384 including nitrate and NO_2), i.e., 0.63 and 0.34, were observed in P2 than those (0.48 and 0.14)

385 in P1. Under stagnant weather conditions (wind speed < 2 m s^{-1}), higher temperatures and RH

386 as shown in Table S4 might facilitate the conversion from precursors into particles (Liu et al.,

387 2020d). The above results indicate that the air pollution dominated by secondary formation is

388 much more serious in P2, which is supported by both the increased concentration and the

389 greater number of pollution days in P2 than in P1, even though primary emissions decreased

390 obviously.

391 **3.2 Influence of Chinese New Year and the COVID-2019 epidemic event on HONO**

392 **concentration in Beijing.**

393 Figure 2 displays the time series of the HONO concentration, the $HONO/NO_2$ ratio, and the

394 traffic index (www.nitrafficindex.com). In Fig. 2b, there is a significant decrease in the traffic

395 index ($P < 0.05$), indicating reduced traffic congestion during the COVID-19 lockdown (P2

396 period) compared to the P1 period. The $HONO/NO_2$ ratio is frequently used to indicate the

397 conversion of NO_2 to HONO through heterogeneous reactions (Sun et al., 2013). A higher

398 $HONO/NO_2$ indicates that the heterogeneous conversion process plays a more significant role

399   in HONO production. However, as depicted in Fig. 2b, both the traffic index and HONO exhibit

400   a similar decreasing trend, while the HONO/NO$_2$ ratio remains relatively stable. Notably, both

401   the traffic index and the NO concentration experienced a steep decline after January 24,

402   coinciding with a significant decrease ($P < 0.05$) in HONO concentration. Furthermore, as

403   shown in Fig. S4, there is a strong correlation between HONO and NO$_x$ in both P1 and P2.

404   However, HONO concentration does not track PM$_{2.5}$ concentration well. These results imply

405   that HONO might be more influenced by vehicle emissions than by heterogeneous reactions

406   on aerosol surfaces. This contrasts with prior studies that heterogeneous reactions on aerosol

407   surfaces are the primary source of HONO in pollution events in Beijing (Liu et al., 2014; Cui

408   et al., 2018; Meng et al., 2020).
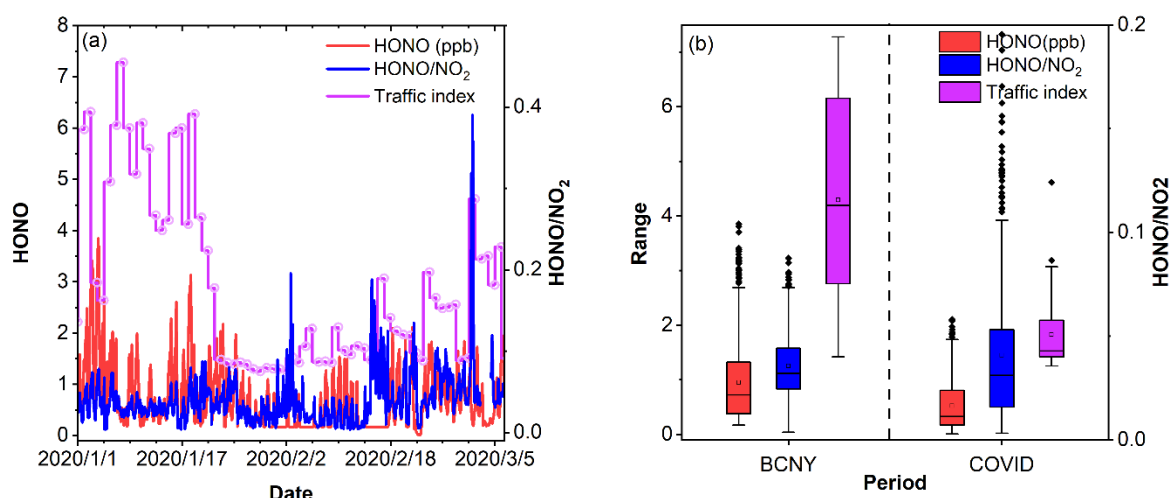
409

410   **Figure 2. (a)** Times series of HONO, traffic index, and HONO/NO$_2$, **(b)** Box plots of HONO,

411   HONO/NO$_2$, and the traffic index in Beijing during different periods (BCNY=P1, LOCK=P2).

412

413   Table S7 summarizes the mean concentrations of HONO, NO$_2$, NO, and PM$_{2.5}$ over the

414   two periods in this study as well as the data reported in previous studies. During P1, HONO

415   concentration ranged from 0.17 to 3.85 ppb, with a mean value of 0.97 ± 0.74 ppb. This

concentration is similar to previous observations, such as in Beijing, Xi'an, Jinan, Shanghai,

Hong Kong, and Rome, which all ranged from 0.95 to 1.15 ppb (Acker et al., 2006; Wang et

al., 2013; Xu et al., 2015; Huang et al., 2017; Liu et al., 2020d; Li et al., 2018). However, during

the COVID-19 lockdown, the HONO concentration decreased to 0.53 ± 0.44 ppb, representing

a drop of 45.3% compared with that in BCNY. After deweather, the HONO concentration

decreased significantly from 0.89 ± 0.37 in P1 to 0.51 ± 0.25 ppb in P2 at a confidence level of

0.05, with a decrease of 42.7%. This means that meteorology has little impact on HONO. This

value is comparable to the concentrations reported in the literature for clean days in December

2016 in Beijing (0.5 ± 0.2 ppb) and in the winter of 2018 in Xiamen (0.52-0.61 ppb). At the

same time, as discussed in the previous section, the NO concentration decreased by nearly 87%

from BCNY to COVID-19 lockdown, and the NO_2 concentration dropped by about 36%.

Consequently, we can conclude that the concentrations of HONO, NO, and NO_2 were the most

affected pollutants during the COVID-19 lockdown period.

Figure 3 shows the diurnal curves of HONO, NO_x, NO, NO_2, $HONO/NO_2$, O_3, SO_2, and

$PM_{2.5} \times NO_2$ during P1 (BCNY) and P2 (COVID-19 lockdown). The black and red lines

represent P1 and P2, respectively. HONO shows a similar trend in both periods. After sunset,

HONO began to accumulate due to the attenuation of solar radiation and the development of

the boundary layer, reaching maximum values of 1.41 ± 0.83 ppb and 0.92 ± 0.64 ppb around

7:00 during P1 and P2, respectively. Subsequently, due to the impact of the boundary layer and

rapid photolysis, the HONO concentration gradually decreased and remained at a low level

until sunset, with the corresponding minimum value of 0.43 ± 0.24 ppb and 0.27 ± 0.17 ppb at

about 15:00. Similar to HONO, the NO_2 concentration shows an upward trend during the

438   morning rush hour. Its peak appeared at 7:00 (BCNY: 31.4 ± 9.23 ppb; COVID-19 lockdown:

439   23.3 ± 10.74 ppb), and then dropped rapidly and remained at a low level due to photochemical

440   processes and the development of the boundary layer. The minimum concentration occurs

441   around 14:00 to 15:00 (BCNY: 18.17 ± 10.69 ppb; COVID-19 lockdown: 11.0 ± 7.64 ppb).

442   After sunset, NO_2 began to increase again. It is worth noting that during BCNY, both NO_2 and

443   NO exhibited a prominent evening peak, whereas there was no such evening peak during the

444   COVID-19 lockdown. Thus, NO_x and NO_2 had similar changing trends, i.e., the morning peak

445   observed in both periods with the highest mean values of 65.93 ± 50.37 ppb and 31.7 ± 21.47

446   ppb in BCNY and COVID-19 lockdown, respectively.

447
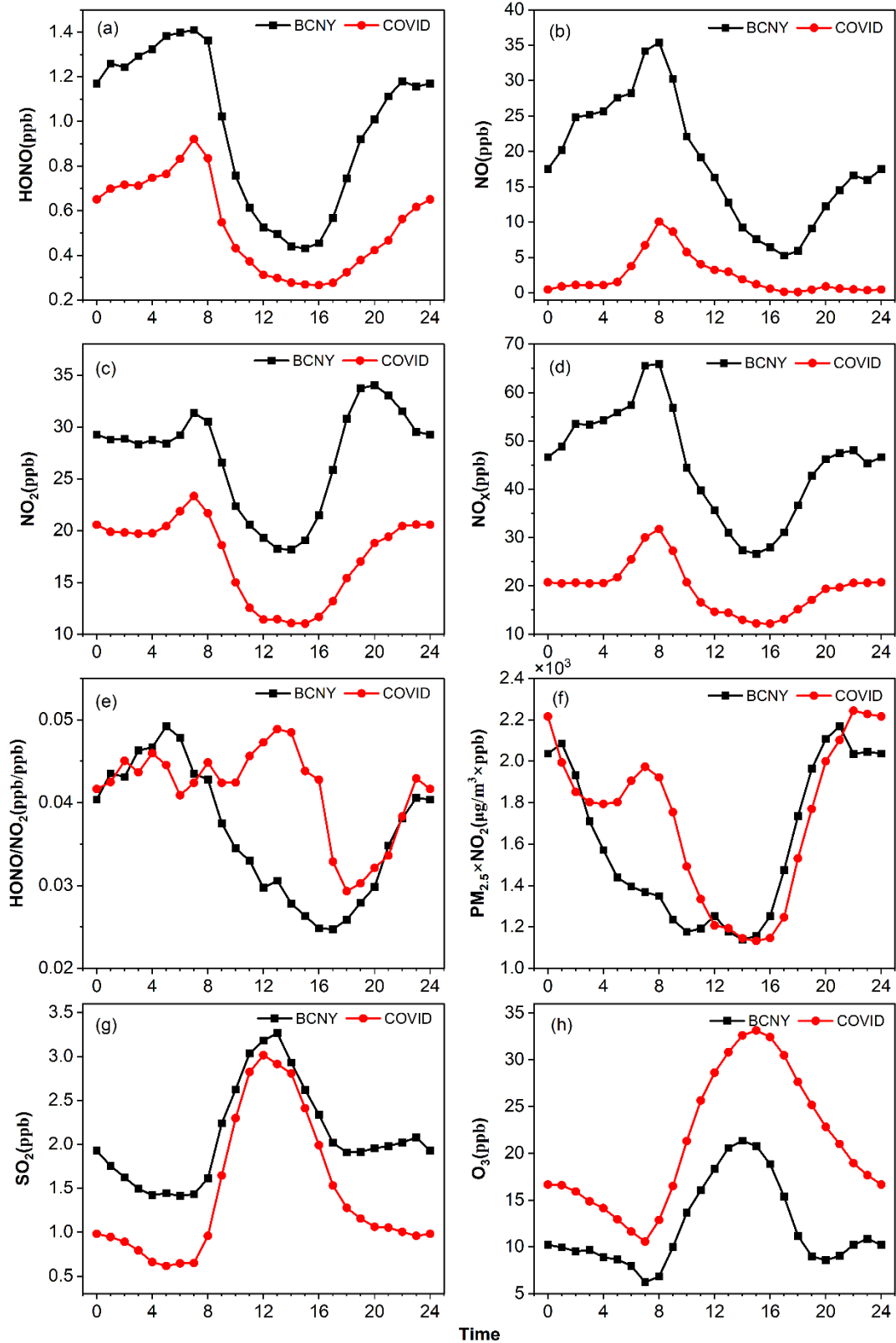
Figure 3. Diurnal variation of HONO, NO, NO$_2$, NO$_x$, HONO/NO$_2$, PM$_{2.5}$×NO$_2$, SO$_2$, O$_3$. The

black lines are the diurnal curves before CNY and the red ones are during the COVID-19

450 lockdown.

451

452 NO and HONO showed a similar trend in P1. They began to decline continuously after

453 sunrise and continued to rise after sunset. The peaks of NO were 35.40 ± 43.55 ppb and $10.0 \pm$

454 12.67 ppb in P1 and P2, respectively. It is worth noting that the upward trend of NO

455 concentration in the afternoon of the P2 stage was not obvious, as the absolute concentration

456 of NO was very low. O_3 and HONO showed opposite diurnal curves, with the maximum O_3

457 concentrations occurring in the afternoon, which were 21.35 ± 9.31 ppb and 33.14 ± 10.26 ppb

458 in P1 and P2, respectively. SO_2 and O_3 exhibited similar trends, with the maximum values in

459 P1 and P2 were 3.26 ± 2.19 ppb and 3.01 ± 3.06 ppb at 13:00, and their lowest values were

460 1.41 ± 0.68 ppb and 0.62 ± 0.82 ppb at 5:00 or 6:00.

461 Previous studies proposed that the heterogeneous reactions of NO_2 on the aerosol surface

462 play an important role in HONO production. Specifically, this pathway was considered the

463 major source of HONO on polluted days (Cui et al., 2018; Meng et al., 2020; Zhang et al.,

464 2020). $PM_{2.5} \times NO_2$ can be used as an indicator for the heterogeneous reaction of NO_2 on the

465 surface of aerosols (Cui et al., 2018). It was found that the value of $PM_{2.5} \times NO_2$ in P2 ($1697 \pm$

466 2142) was slightly higher than that in P1 (1583 ± 1967). In the early morning, the product of

467 $PM_{2.5}$ and NO_2 in the P2 stage was even higher than that in the P1 stage. On the other hand, the

468 ratio of $HONO/NO_2$ is usually used to evaluate the formation of HONO during the conversion

469 of NO_2. As shown in Fig. 3, in the P1 stage, the $HONO/NO_2$ ratio shows a similar daily trend

470 to HONO, which began to rise after sunset and reached a peak at night and then decreased in

471 the early morning due to the increase of NO_2 concentrations and the photolysis of HONO. In

472   the P2 stage, the variation of HONO/NO$_2$ is different from that of the P1. The HONO/NO$_2$ in

473   the P2 period was higher than that in the P1 stage, especially in the daytime, although the values

474   of HONO/NO$_2$ in both stages (P1: 0.036 ± 0.016; P2: 0.041 ± 0.038) were lower than that

475   (0.052-0.080) reported by Cui et al (Cui et al., 2018). Subsequently, we further analyzed

476   HONO$_{corr}$/NO$_2$ (details shown in Sect. 2.2). The HONO$_{corr}$/NO$_2$ attributed to secondary

477   formation via heterogeneous reactions changed obviously after subtracting other secondary

478   HONO sources. As shown in Fig. S5, the daytime peak of HONO$_{corr}$/NO$_2$ in P2 became more

479   prominent compared with that in Fig. 3e, while the daytime (8:00 - 18:00) HONO$_{corr}$/NO$_2$

480   (0.022 ± 0.014) in P1 was significantly (P < 0.05) lower than that in P2 (0.040 ± 0.053).

481   However, the HONO concentration decreased significantly as discussed above. These results

482   suggest that heterogeneous reactions of NO$_2$ on the aerosol surfaces may not be a major source

483   of HONO because the enhanced potential of heterogeneous reactions indicated by PM$_{2.5}$×NO$_2$

484   and HONO$_{corr}$/NO$_2$ in P2 contrast with the decreased HONO concentrations compared to P1.

485   In summary, we propose that during our observation period, heterogeneous reactions of NO$_2$

486   should have a relatively minor contribution to HONO production.

487   **3.3 Relative change of different sources to HONO budget in Beijing during different**

488   **periods.**

489   Figure 4a-f shows the diurnal variation of HONO production or emission rates for these sources

490   at different stages, and Fig. 4g-l shows the budget of the HONO sources and sinks during P1

491   (BCNY) and P2 (COVID-19 lockdown). The HONO production rate via homogeneous

492   reaction between NO and OH in the P1 period was much higher than that in the P2 period,

493   especially during the daytime. The average rate decreased from 0.145 ± 0.189 ppb h^{-1} in the P1

494 stage to 0.047 $\pm$ 0.073 ppb h^{-1} in the P2 stage. The OH concentrations increased slightly from

495 P1 ($4.1\times10^5 \pm 5.8\times10^5$ cm^{-3}) to P2 ($6.7\times10^5 \pm 1.0\times10^6$ cm^{-3}). Therefore, the observed decrease

496 in HONO production rate via homogeneous reaction between NO and OH should be ascribed

497 to the substantial reduction of NO concentration as discussed above. It can be seen that the

498 homogeneous reaction between NO and OH is indeed an important source of HONO at night.

499 In previous studies, the nocturnal production of HONO via NO and OH was often ignored

500 because low nighttime OH concentrations were estimated (Fu et al., 2019). However, some

501 studies have shown that the observed nighttime OH concentrations in the Beijing urban area

502 can also be maintained in the order of 10^5 molecules cm^{-3} in winter, which also means that the

503 contribution of the reaction channels of NO and OH to HONO cannot be ignored. In the P1

504 stage, the homogeneous reaction between NO and OH accounted for $13 \pm 5\%$ of the nighttime

505 HONO sources. However, in the daytime, the homogeneous reaction between NO and OH was

506 the most important source of HONO, which accounted for up to $51 \pm 32\%$ of the daytime

507 HONO source. This is consistent with previous studies in urban Beijing (Gu et al., 2021; Jia et

508 al., 2020; Liu et al., 2021). Interestingly, a recent study proposed a new mechanism through

509 smog chamber experiments, that is, NOx photooxidation (reaction of NO and adsorbed HNO$_3$)

510 may be an important daytime HONO source (Song et al., 2023), although it has not yet been

511 verified by field observations. In the P2 stage, its proportion in the night was negligible due to

512 the dramatic decrease in NO concentration during the pandemic event, and the maximal

513 proportion of HONO sources in the daytime was also reduced to $25 \pm 14\%$. It is worth noting

514 that the parameterization of OH concentration will introduce uncertainty to HONO sources.

515 Table S3 shows the sensitivity test for the HONO simulation. An increase of 10% and 200% in

OH concentration in M3 and M4 results in a 24-26% change in the HONO source. It means that the accuracy of the OH measurement is important for understanding the source-sink balance of the HONO.
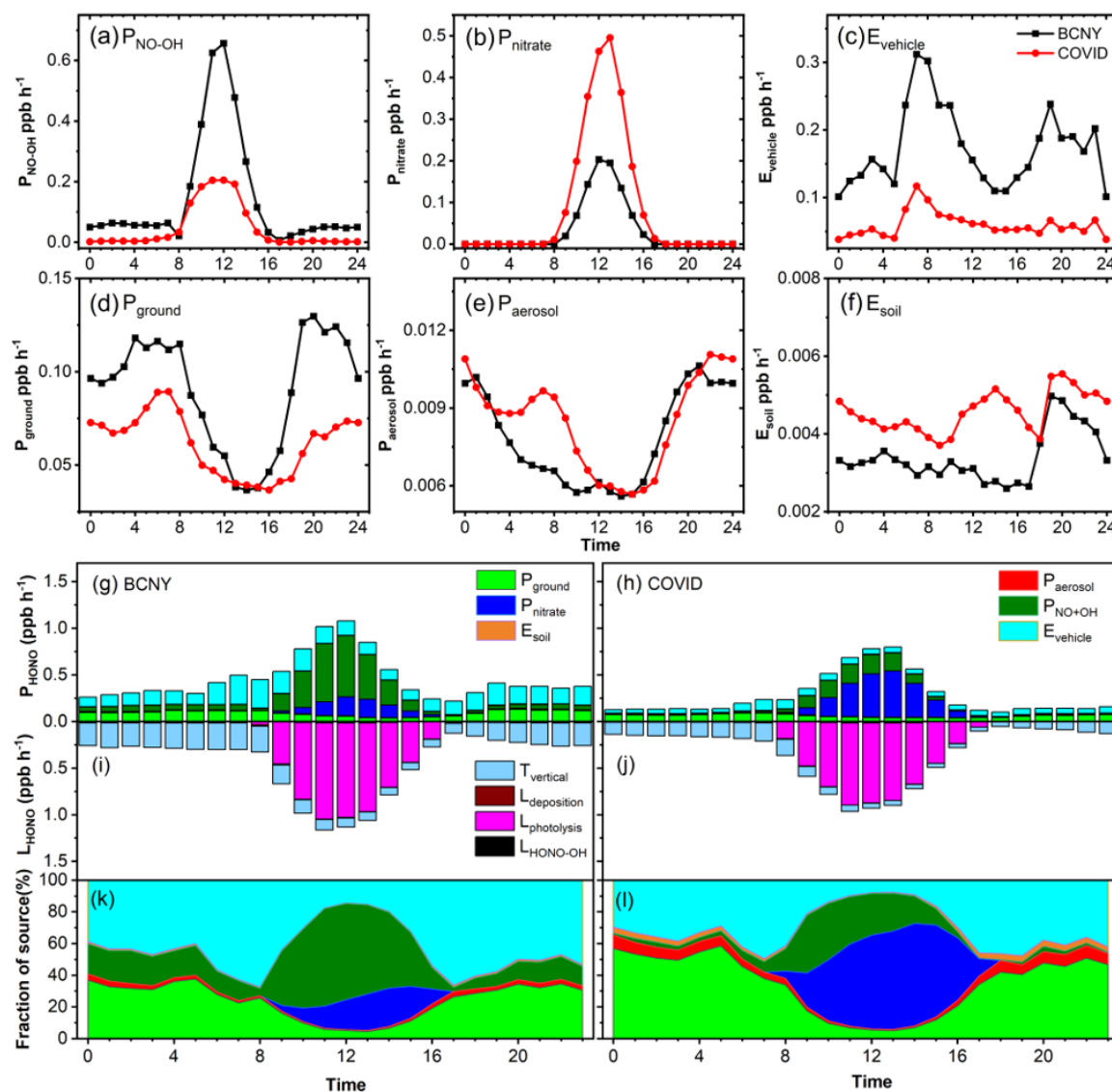

Figure 4. (**a-f**): Diurnal variations in HONO production rate from various sources. The black lines are the diurnal curves before CNY and the red ones are during the COVID-19 lockdown. (**g-l**): Variations of HONO budget. (**g,h**) Diurnal production rates of HONO; (**i,j**) loss rates of HONO (unit: ppb h^{-1}); (**k,l**) relative contributions of each source. Panels (**g**),(**i**), and (**k**) show the data from BCNY, and panels (**h**),(**j**), and (**l**) show the data from the COVID-19 lockdown.

525   The daytime HONO source related to photolysis of nitrate (0.223 ± 0.175 ppb h^{-1}) in the

526   P2 stage was much larger than that (0.107 ± 0.068 ppb h^{-1}) in the P1 stage. It contributed $16 \pm$

527   10% to the daytime HONO source in the P1 period. However, it became the most important

528   daytime source of HONO in the P2 stage, accounting for up to $53 \pm 41\%$, as both the nitrate

529   concentration and the light intensity increased significantly ($P < 0.05$). Ye et al. (Ye et al., 2016)

530   reported that the photolysis rate constants of nitrate particles on the surface of different

531   materials were in the range of 6.0×10^{-6} - 3.7×10^{-4} s^{-1}. Thus, we used the lower limit value of

532   6.0×10^{-6} s^{-1} and the upper limit value of 3.7×10^{-4} s^{-1} for sensitivity tests (methods M9 and M10),

533   which resulted in a change of 25% and 95% of HONO sources, respectively.

534   The direct emission rate of HONO from vehicles in the P1 stage was much higher than

535   that in the P2 stage. The emission rate of the P1 stage was between 0.135-0.39 ppb h^{-1}, with a

536   mean value of 0.227 ± 0.071 ppb h^{-1}. This is comparable with the value (0.079-0.32 ppb h^{-1}) in

537   the winter of 2018 (Liu et al., 2020d). In the P2 stage, it decreased to 0.062-0.173 ppb h^{-1}, with

538   a mean value of 0.086 ± 0.027 ppb h^{-1}. This value is slightly higher than the lower limit of

539   vehicle emissions of 0.013-0.076 ppb h^{-1} estimated using an emission factor of 0.18% in our

540   previous study (Liu et al., 2020d), while it is less than the upper limit reported by Li (Li et al.,

541   2018) in Jinan of 0.13 ± 0.06-0.53 ± 0.23 ppb h^{-1}. During the lockdown, the emission rate of

542   HONO from vehicles was reduced by 53%-66% when compared with that before the lockdown.

543   In the P1 period, vehicle emission was an important nighttime source of HONO. It contributed

544    $53 \pm 17\%$ to the HONO sources, much higher than heterogeneous reactions of NO_2 on aerosol

545   and ground surfaces (33%) (Fig. S9). In the P2 stage, due to the reduction of transport, the

546   contribution of vehicle emissions to HONO sources decreased to $40 \pm 14\%$, while the

547 contribution of heterogeneous reactions of NO_2 increased to 53%. This is consistent with the

548 observed decrease in HONO concentrations. The daytime contributions of vehicle emissions

549 to HONO sources were lower than the corresponding nighttime contributions, while it was still

550 higher in the P1 period than in the P2 period. These results mean that vehicles should be

551 important contributors to ambient HONO under typical emission patterns in Beijing. In the

552 sensitivity analysis, the emission factors of 0.008 and 0.0186 were considered in methods M1

553 and M2, and 8% and 20% changes were found in the simulated HONO sources, respectively.

554 The yield of soil emissions in the P2 stage is also higher than that in the P1 stage due to the

555 temperature rise in the P2 stage because the temperature will affect the soil emission flux

556 (Oswald et al., 2013), while the importance of this source is negligible in this study. In M15

557 and M16, we amplify and shrink the soil emission flux by 10 times, respectively, and the change

558 of the simulated HONO sources was less than 5%.

559 As shown in Fig. 4e, the heterogeneous reaction rate of NO_2 on aerosols did not change

560 much between the P1 and P2 stages. The average production rate of HONO in the P1 stage was

561 0.007 ± 0.002 ppb h^{-1}, and it was 0.008 ± 0.002 ppb h^{-1} in the P2 stage, showing an increase of

562 about 14%. It is worth noting that the HONO formation rate from the heterogeneous conversion

563 of NO_2 on the surface of aerosol does not decrease, which is caused by the increase in $PM_{2.5}$

564 concentration along with a decrease in NO_2 concentration during the P2 period. If the

565 heterogeneous transformation of NO_2 on particulate surfaces is important, especially in the case

566 of heavy pollution, increased HONO concentrations should be expected instead of a large

567 decrease, as observed in the P2 stage. This is consistent with the changes in $HONO_{corr}/NO_2$ and

568 $PM_{2.5} \times NO_2$ as discussed in Sect. 3.2. For the heterogeneous transformation of NO_2 on the

569   ground and aerosol surfaces, this source is sensitive to the uptake coefficient (γ) of NO_2. For

570   the aerosol surface, here we assume that the upper limit of γ is 10^{-5} (M7) and the lower limit is

571   2×10^{-7} (M8) (Liu et al., 2019b; Liu et al., 2020d). As shown in Table S3, the change in simulated

572   HONO is less than 5%. We reduced and magnified the surface area concentration (A_s) of

573   particulate matter by a factor of 10 in M11 and M12, respectively, and the resulting change in

574   HONO was still less than 10%. It should be noted that HONO is sensitive to the uptake

575   coefficient and surface area concentration. When the uptake coefficient is expanded by 5 times

576   or reduced by 10 times, the absolute HONO flux attributed to heterogeneous reactions increases

577   5 times or decreases 10 times, while the relative contribution is very low due to the small

578   absolute value of heterogeneous reactions compared with other sources.

579   Regarding the heterogeneous reaction of NO_2 on ground surfaces, the average formation

580   rate of HONO in the P1 stage was 0.09 ± 0.03 ppb h^{-1}, while it was 0.06 ± 0.02 ppb h^{-1} in the

581   P2 stage. This is ascribed to the significant drop ($P < 0.05$) in NO_2 concentration during the

582   COVID-19 lockdown. Fig. 4k shows that the heterogeneous reaction of NO_2 on ground

583   surfaces is also an important nighttime source of HONO. In the P1 stage, heterogeneous

584   reactions on both aerosol and ground surfaces explained 33% of the nighttime HONO source.

585   In the daytime, however, the contribution of heterogeneous reactions to HONO sources

586   dropped rapidly. In the P2 stage, the heterogeneous reaction became the most important

587   nighttime source contributing up to 53% of HONO (Fig. S9). This can be explained by the

588   significant decrease ($P < 0.05$) in NO and direct emissions of HONO from traffic. Similar to

589   heterogeneous reactions on aerosol surfaces, we assumed that the upper limit of γ_{NO2} on

590   ground surfaces was 10^{-5} (M5) and the lower limit was 2×10^{-7} (M6), respectively, and the

591   changes in simulated HONO source were 40% and 9%, respectively. Indicating that HONO is

592   sensitive to the NO_2 uptake coefficient on the ground surface. In M13 and M14, we set the

593   surface roughness (δ) to 1 and 2.2 as reported in the literature, respectively (Zhang et al., 2022b;

594   Liu et al., 2020c), and the simulated changes in HONO were less than 8%.

595   During the P1 and P2 periods, the mean values of $T_{vertical}$ were 0.195 ± 0.076 ppb h^{-1} and

596   0.102 ± 0.048 ppb h^{-1}, respectively. It was the main sink of HONO at night. The mean $L_{photolysis}$

597   was 0.563 ± 0.375 ppb h^{-1} and 0.442 ± 0.324 ppb h^{-1}, respectively, which was the main daytime

598   sink of HONO. The average loss rate of $L_{HONO-OH}$ during P1 and P2 was 0.005 ppb h^{-1} and

599   0.004 ppb h^{-1}, respectively. The $L_{deposition}$ was 0.009 ± 0.005 ppb h^{-1} during P1, while it was

600   0.004 ± 0.003 ppb h^{-1} during P2. In M17 and M18, we set the lower limit of the deposition rate

601   (V_d) to 0.00077 and the upper limit to 0.025 (Zhang et al., 2023b), causing a change of 1% and

602   24% in the simulated HONO, respectively. In M19 and M20 at the same time, we set the

603   dilution rate ($K_{dilution}$) to 0.1 and 0.44, resulting in a 12% and 19% change, respectively.

604   It should be noted that each source is sensitive to the corresponding parameter as discussed

605   above. Thus, a more restrictive criterion is required to evaluate the reasonability of the

606   parameterization. We further estimated the HONO concentration according to Eq. (2) and the

607   parameters described in Sect. 2.2 to verify these calculated sources and sinks of HONO. Fig.

608   S6 shows the time series of estimated HONO concentrations. The observed HONO

609   concentrations were also shown for comparison. The estimated HONO concentrations were

610   well correlated with the observed values from the perspective of both diurnal curves and the

611   scattering point plot during the whole period (Fig. S7 and Fig. S8) although the estimated

612   HONO concentrations were slightly lower than the observed values at noon as shown in Fig.

S7. This means that our parametric scheme is overall reasonable but still underestimates the daytime HONO source due to some unknown daytime sources. This unknown source may be related to the photochemical reactions related to NO_2 and nitroaromatic compounds mentioned in recent studies (Liu et al., 2020a). Liu et al. have found the photoenhanced effect of the conversion from NO_2 to HONO on real urban grime and glass windows simulated in laboratory studies (Liu et al., 2019a; Liu et al., 2020b). Yang et al. also have proposed that photolysis of nitroaromatic compounds may be a daytime source of HONO (Yang et al., 2021). Considering the uncertainty of parameterization, we used Oracle Crystal Ball (version 11.1.2.4, Oracle's software for modeling, prediction, simulation, and optimization) (Rahmani et al., 2023) to evaluate the overall uncertainty of the parameterization through Monte Carlo simulations. The relative standard deviation is 27.2% for the HONO budget (details are in SI).

In summary, heterogeneous reactions of NO_2 (including ground and aerosol surfaces) contributed 33% to the nocturnal HONO sources in the P1 stage, while they increased to 53% in the P2 stage. Ground surfaces were the main interfaces for heterogeneous reactions, compared to aerosol surfaces. At the same time, vehicle emissions account for $53 \pm 17\%$ and $40 \pm 14\%$ of nighttime HONO sources in the P1 and P2 stages, respectively. To explore whether meteorological factors have an impact on the sources of HONO, we conducted the budget analysis of HONO using the deweathered pollutant concentrations. The results are shown in Fig. S10. When compared with the sources of HONO calculated using the raw concentration dataset (Fig. S9), it can be seen that deweathering has little effect on the daytime sources of HONO. For the nighttime source of HONO, however, deweathering caused the proportion of traffic emissions during BCNY increasing from 53% to 63% before the CNY or from 40% to

635　45% during the COVID-19 lockdown. The contribution of heterogeneous reactions of NO_2 on

636　ground surfaces decreased from 31% to 19% before the CNY or from 47% to 42% during the

637　COVID-19 lockdown. These results further highlight the importance of vehicle emissions to

638　nocturnal HONO sources in Beijing.

639　　　Therefore, regardless of whether the impact of meteorological conditions on the source of

640　HONO is considered, we can conclude that traffic-related emissions, rather than heterogeneous

641　reactions of NO_2 were the main HONO source at night in Beijing in the typical emission

642　patterns of air pollutants.

643　**4. Conclusions and atmospheric implications**.

644　During the COVID-19 pandemic at the beginning of 2020, the concentration of many air

645　pollutants decreased significantly ($P < 0.05$) due to the emission reduction of factories and

646　transportation. The average concentration of NO_x decreased by about 57%, of which NO

647　decreased by about 87%, and NO_2 decreased by about 36%. The average concentration of

648　HONO decreased by about 45.3% compared with those before the pandemic control. The

649　average concentration of O_3 and $PM_{2.5}$ increased by approximately 75% and 50%, respectively.

650　It is worth noting that in addition to primary emissions, meteorological changes will also affect

651　changes in atmospheric pollutant concentrations. After removing meteorological factors, the

652　change proportions of $PM_{2.5}$ concentration in the two stages were -4.3% and -2.3% respectively.

653　The HONO changes were -8.3% and -3.8% respectively, the CO changes were -9.3% and -6.2%

654　respectively, and the SO_2 changes were +8.6% and +0.7% respectively. The change proportions

655　are all less than 10%, which means that the impact of changes in meteorological factors on

656　$PM_{2.5}$, HONO, CO, and SO_2 is very weak. However, the change proportions of NO in the two

657 stages were -16.2% and +32.8%, respectively, and O_3 was +39.6% and +6.2% respectively.

658 The change ratio is greater than 30%, indicating that NO and O_3 are greatly affected by

659 meteorology. In addition, the changes in NO_2 were -13.8% and -4.8% respectively, implying

660 that NO_2 is also affected by meteorological factors. From the entire observation period, except

661 for O_3, the changes of other species in the two periods fluctuated between 2.3% and 7.8% after

662 deweather, all less than 8%. In general, after removing the meteorological effects, NO

663 increased by 79%, NO_2 increased by approximately 29%, HONO decreased by approximately

664 43%, and $PM_{2.5}$ increased by approximately 50%. It is worth noting that O_3 increased by about

665 33%, which is much lower than the change in observed values (75.1%) (as shown in Table S6).

666 Although we have tried to assess the impact of meteorological factors quantitatively, this still

667 carries some uncertainty. In particular, uncertainty is inevitable for the source assessment of

668 substances such as HONO that are affected by a large number of parameters.

669   In this study, the parameters of HONO sources were optimized. The balance of sources

670 and sinks is well supported by a relatively high correlation between observed and estimated

671 HONO concentrations. During the observation period, we used lockdown during COVID-19

672 as a disturbance factor and compared the concentration and source changes of HONO before

673 and during COVID-19 lockdown to determine whether heterogeneous reactions on the surface

674 of particulate matter and vehicle emissions were important HONO sources. We found that

675 vehicle-related emissions were the most important nighttime HONO source in Beijing,

676 contributing 50-60% to the nighttime HONO sources. The homogeneous reaction between NO

677 and OH and the heterogeneous reaction of NO_2 on the aerosol surface were not important for

678 the contribution of nocturnal HONO, accounting for $13 \pm 5\%$ and $2 \pm 1\%$, respectively. The

679　heterogeneous reaction of NO_2 on ground surfaces was also found to be an important source of

680　HONO at night, accounting for $31 \pm 5\%$ of the nighttime HONO sources. Nitrate photolysis

681　became the most important source of HONO during the daytime compared with the situation

682　before the pandemic control because of the combined effect of the increase in the average

683　concentration of nitrate and the decrease in the NO concentration during the pandemic. We

684　conducted a potential source contribution function (PSCF, Fig S2) analysis in different periods,

685　i.e., BCNY and COVID, at the BUCT station and further compared the PSCF of HONO at

686　BUCT station with that at the Institute Atmospheric Physics (IAP) station, which is around 8

687　km from BUCT station, from January 24, 2022, to January 31, 2022, when the data were

688　available. The PSCF patterns were highly similar in different periods or locations. These results

689　mean that the air mass should be consistent during the COVID-19 lockdown and BCNY and

690　HONO should be evenly distributed in Beijing. Thus, the impact of meteorological changes on

691　the accuracy of observations cannot be ruled out, which is also a limitation of this study, but its

692　influence should be comparable between BCNY and the COVID lockdown. And the

693　conclusions drawn based on the observations at BUCT should represent the situation in Beijing.

694　Through uncertainty assessment, it was found that the assumption of J_{NO3^-} would have the

695　greatest uncertainty, with a standard deviation of $\pm 19\%$. Nevertheless, this study confirms that

696　reducing anthropogenic emissions can indeed reduce the concentration of HONO in the

697　atmosphere. However, such reduction does not have a simple linear relation with the reduction

698　in human activities, but it also depends on meteorological conditions and complex chemical

699　transformation processes taking place in the atmosphere.

700　　　As a megacity in China, Beijing has a large population and intensive traffic emissions, as

701   a result of frequent air pollution. Although concentrations of HONO are usually lower than

702   those of other major pollutants, HONO efficiently triggers the formation of secondary

703   pollutants acting as an important primary source of OH radicals. Therefore, the sources of

704   HONO deserve to be investigated for air pollution control in Beijing. Our results suggest that

705   motor vehicle emissions are an important HONO source, while the contribution of the

706   heterogeneous conversion of NO_2 to HONO on the aerosol surfaces still needs to be further

707   evaluated and, especially, the kinetic parameters on ambient aerosol should be determined. In

708   future research, it is necessary to combine field observations, laboratory studies, and model

709   simulations to quantify the contribution of traffic-related emissions to HONO, and finally

710   obtain an accurate budget of HONO.

References

Acker, K., Febo, A., Trick, S., Perrino, C., Bruno, P., Wiesen, P., Möller, D., Wieprecht, W., Auel, R., Giusto, M., Geyer, A., Platt, U., and Allegrini, I.: Nitrous acid in the urban area of Rome, Atmospheric Environment, 40, 3123-3133, 10.1016/j.atmosenv.2006.01.028, 2006.

Alicke, B.: Impact of nitrous acid photolysis on the total hydroxyl radical budget during the Limitation of Oxidant Production/Pianura Padana Produzione di Ozono study in Milan, Journal of Geophysical Research, 107, 10.1029/2000jd000075, 2002.

Bond, A. M. H., Frey, M. M., Kaiser, J., Kleffmann, J., Jones, A. E., and Squires, F. A.: Snowpack nitrate photolysis drives the summertime atmospheric nitrous acid (HONO) budget in coastal Antarctica, Atmospheric Chemistry and Physics, 23, 5533-5550, 10.5194/acp-23-5533-2023, 2023.

Chai, J., Dibb, J. E., Anderson, B. E., Bekker, C., Blum, D. E., Heim, E., Jordan, C. E., Joyce, E. E., Kaspari, J. H., Munro, H., Walters, W. W., and Hastings, M. G.: Isotopic evidence for dominant secondary production of HONO in near-ground wildfire plumes, Atmospheric Chemistry and Physics, 21, 13077-13098, 10.5194/acp-21-13077-2021, 2021.

Chen, Y., Wang, W., Lian, C., Peng, C., Zhang, W., Li, J., Liu, M., Shi, B., Wang, X., and Ge, M.: Evaluation and impact factors of indoor and outdoor gas-phase nitrous acid under different environmental conditions, J Environ Sci (China), 95, 165-171, 10.1016/j.jes.2020.03.048, 2020.

Crilley, L. R., Kramer, L. J., Ouyang, B., Duan, J., Zhang, W., Tong, S., Ge, M., Tang, K., Qin, M., Xie, P., Shaw, M. D., Lewis, A. C., Mehra, A., Bannan, T. J., Worrall, S. D., Priestley, M., Bacak, A., Coe, H., Allan, J., Percival, C. J., Popoola, O. A. M., Jones, R. L., and Bloss, W. J.: Intercomparison of nitrous acid (HONO) measurement techniques in a megacity (Beijing), Atmos. Meas. Tech., 12, 6449-6463, 10.5194/amt-12-6449-2019, 2019.

Cui, L., Li, R., Zhang, Y., Meng, Y., Fu, H., and Chen, J.: An observational study of nitrous acid (HONO) in Shanghai, China: The aerosol impact on HONO formation during the haze episodes, Sci Total Environ, 630, 1057-1070, 10.1016/j.scitotenv.2018.02.063, 2018.

Cui, Y., Ji, D., Maenhaut, W., Gao, W., Zhang, R., and Wang, Y.: Levels and sources of hourly PM2.5-related elements during the control period of the COVID-19 pandemic at a rural site between Beijing and Tianjin, Sci Total Environ, 744, 140840, 10.1016/j.scitotenv.2020.140840, 2020.

Dillon, M. B., Lamanna, M. S., Schade, G. W., Goldstein, A. H., and Cohen, R. C.: Chemical evolution of the Sacramento urban plume: Transport and oxidation, Journal of Geophysical Research: Atmospheres, 107, ACH 3-1-ACH 3-15, 10.1029/2001jd000969, 2002.

Ehhalt, D. H. and Rohrer, F.: Dependence of the OH concentration on solar UV, Journal of Geophysical Research: Atmospheres, 105, 3565-3571, 10.1029/1999jd901070, 2000.

Farren, N. J., Ramirez, N., Lee, J. D., Finessi, E., Lewis, A. C., and Hamilton, J. F.: Estimated Exposure Risks from Carcinogenic Nitrosamines in Urban Airborne Particulate Matter, Environ Sci Technol, 49, 9648-9656, 10.1021/acs.est.5b01620, 2015.

Fu, X., Wang, T., Zhang, L., Li, Q., Wang, Z., Xia, M., Yun, H., Wang, W., Yu, C., Yue, D., Zhou, Y., Zheng, J., and Han, R.: The significant contribution of HONO to secondary pollutants during a severe winter pollution event in southern China, Atmospheric Chemistry and Physics, 19, 1-14, 10.5194/acp-19-1-2019, 2019.

Ge, S., Wang, G., Zhang, S., Li, D., Xie, Y., Wu, C., Yuan, Q., Chen, J., and Zhang, H.: Abundant NH3 in China Enhances Atmospheric HONO Production by Promoting the Heterogeneous Reaction of SO2 with NO2, Environ Sci Technol, 53, 14339-14347, 10.1021/acs.est.9b04196, 2019.

Gu, R., Shen, H., Xue, L., Wang, T., Gao, J., Li, H., Liang, Y., Xia, M., Yu, C., Liu, Y., and Wang, W.: Investigating the sources of atmospheric nitrous acid (HONO) in the megacity of Beijing, China, Science of The Total

781 Environment, 10.1016/j.scitotenv.2021.152270, 2021.

782 Han, C., Liu, Y., and He, H.: Role of organic carbon in heterogeneous reaction of NO2 with soot, Environ Sci
783 Technol, 47, 3174-3181, 10.1021/es304468n, 2013.

784 Han, C., Liu, Y., and He, H.: Heterogeneous reaction of NO2 with soot at different relative humidity, Environ Sci
785 Pollut Res Int, 24, 21248-21255, 10.1007/s11356-017-9766-y, 2017a.

786 Han, C., Yang, W., Wu, Q., Yang, H., and Xue, X.: Heterogeneous Photochemical Conversion of NO2 to HONO
787 on the Humic Acid Surface under Simulated Sunlight, Environ Sci Technol, 50, 5017-5023,
788 10.1021/acs.est.5b05101, 2016.

789 Han, X., Zhang, M., Skorokhod, A., and Kou, X.: Modeling dry deposition of reactive nitrogen in China with
790 RAMS-CMAQ, Atmospheric Environment, 166, 47-61, 10.1016/j.atmosenv.2017.07.015, 2017b.

791 Hao, Q., Jiang, N., Zhang, R., Yang, L., and Li, S.: Characteristics, sources and reactions of nitrous acid during
792 winter in the core city of the Central Plains Economic Region in China via high-time-resolution online,
793 Atmospheric Chemistry and Physics Discussions, 10.5194/acp-2019-916, 2019.

794 Huang, R. J., Yang, L., Cao, J., Wang, Q., Tie, X., Ho, K. F., Shen, Z., Zhang, R., Li, G., Zhu, C., Zhang, N., Dai,
795 W., Zhou, J., Liu, S., Chen, Y., Chen, J., and O'Dowd, C. D.: Concentration and sources of atmospheric nitrous
796 acid (HONO) at an urban site in Western China, Sci Total Environ, 593-594, 165-172,
797 10.1016/j.scitotenv.2017.02.166, 2017.

798 Jia, C., Tong, S., Zhang, W., Zhang, X., Li, W., Wang, Z., Wang, L., Liu, Z., Hu, B., Zhao, P., and Ge, M.: Pollution
799 characteristics and potential sources of nitrous acid (HONO) in early autumn 2018 of Beijing, Sci Total Environ,
800 735, 139317, 10.1016/j.scitotenv.2020.139317, 2020.

801 Jiang, Y., Xue, L., Shen, H., Dong, C., Xiao, Z., and Wang, W.: Dominant Processes of HONO Derived from
802 Multiple Field Observations in Contrasting Environments, Environmental Science & Technology Letters, 9, 258-
803 264, 10.1021/acs.estlett.2c00004, 2022.

804 Kanaya, Y., Cao, R., Akimoto, H., Fukuda, M., Komazaki, Y., Yokouchi, Y., Koike, M., Tanimoto, H., Takegawa,
805 N., and Kondo, Y.: Urban photochemistry in central Tokyo: 1. Observed and modeled OH and HO2radical
806 concentrations during the winter and summer of 2004, Journal of Geophysical Research, 112,
807 10.1029/2007jd008670, 2007.

808 Kim, M. and Or, D.: Microscale pH variations during drying of soils and desert biocrusts affect HONO and NH3
809 emissions, Nat Commun, 10, 3944, 10.1038/s41467-019-11956-6, 2019.

810 Kramer, L. J., Crilley, L. R., Adams, T. J., Ball, S. M., Pope, F. D., and Bloss, W. J.: Nitrous acid (HONO)
811 emissions under real-world driving conditions from vehicles in a UK road tunnel, Atmospheric Chemistry and
812 Physics, 20, 5231-5248, 10.5194/acp-20-5231-2020, 2020.

813 Kroll, J. H., Heald, C. L., Cappa, C. D., Farmer, D. K., Fry, J. L., Murphy, J. G., and Steiner, A. L.: The complex
814 chemical effects of COVID-19 shutdowns on air quality, Nat Chem, 12, 777-779, 10.1038/s41557-020-0535-z,
815 2020.

816 Kulmala, M. and Petäjä, T.: Soil Nitrites Influence Atmospheric Chemistry, Science 333, 1586-1587, 2011.

817 Le, T., Wang, Y., Liu, L., Yang, J., Yung, Y. L., Li, G., and Seinfeld, J. H.: Unexpected air pollution with marked
818 emission reductions during the COVID-19 outbreak in China, Science, 369, 702-+, 10.1126/science.abb7431,
819 2020.

820 Li, D., Xue, L., Wen, L., Wang, X., Chen, T., Mellouki, A., Chen, J., and Wang, W.: Characteristics and sources
821 of nitrous acid in an urban atmosphere of northern China: Results from 1-yr continuous observations, Atmospheric
822 Environment, 182, 296-306, 10.1016/j.atmosenv.2018.03.033, 2018.

823 Li, S., Song, W., Zhan, H., Zhang, Y., Zhang, X., Li, W., Tong, S., Pei, C., Wang, Y., Chen, Y., Huang, Z., Zhang,
824 R., Zhu, M., Fang, H., Wu, Z., Wang, J., Luo, S., Fu, X., Xiao, S., Huang, X., Zeng, J., Zhang, H., Chen, D.,

Gligorovski, S., Ge, M., George, C., and Wang, X.: Contribution of Vehicle Emission and NO2 Surface Conversion to Nitrous Acid (HONO) in Urban Environments: Implications from Tests in a Tunnel, Environ Sci Technol, 10.1021/acs.est.1c00405, 2021.

Li, X., Brauers, T., Häseler, R., Bohn, B., Fuchs, H., Hofzumahaus, A., Holland, F., Lou, S., Lu, K. D., Rohrer, F., Hu, M., Zeng, L. M., Zhang, Y. H., Garland, R. M., Su, H., Nowak, A., Wiedensohler, A., Takegawa, N., Shao, M., and Wahner, A.: Exploring the atmospheric chemistry of nitrous acid (HONO) at a rural site in Southern China, Atmospheric Chemistry and Physics, 12, 1497-1513, 10.5194/acp-12-1497-2012, 2012.

Liang, Y., Zha, Q., Wang, W., Cui, L., Lui, K. H., Ho, K. F., Wang, Z., Lee, S. C., and Wang, T.: Revisiting nitrous acid (HONO) emission from on-road vehicles: A tunnel study with a mixed fleet, J Air Waste Manag Assoc, 67, 797-805, 10.1080/10962247.2017.1293573, 2017.

Liao, S., Zhang, J., Yu, F., Zhu, M., Liu, J., Ou, J., Dong, H., Sha, Q., Zhong, Z., Xie, Y., Luo, H., Zhang, L., and Zheng, J.: High Gaseous Nitrous Acid (HONO) Emissions from Light-Duty Diesel Vehicles, Environ Sci Technol, 55, 200-208, 10.1021/acs.est.0c05599, 2021.

Liu, J., Deng, H., Lakey, P. S. J., Jiang, H., Mekic, M., Wang, X., Shiraiwa, M., and Gligorovski, S.: Unexpectedly High Indoor HONO Concentrations Associated with Photochemical NO2 Transformation on Glass Windows, Environmental Science & Technology, 54, 15680-15688, 10.1021/acs.est.0c05624, 2020a.

Liu, J., Li, S., Mekic, M., Jiang, H., Zhou, W., Loisel, G., Song, W., Wang, X., and Gligorovski, S.: Photoenhanced Uptake of NO2 and HONO Formation on Real Urban Grime, Environmental Science & Technology Letters, 6, 413-417, 10.1021/acs.estlett.9b00308, 2019a.

Liu, J., Deng, H., Li, S., Jiang, H., Mekic, M., Zhou, W., Wang, Y., Loisel, G., Wang, X., and Gligorovski, S.: Light-enhanced heterogeneous conversion of NO2 to HONO on solid films consisted of fluorene and fluorene/Na2SO4: An impact on urban and indoor atmosphere, Environ Sci Technol, 10.1021/acs.est.0c02627, 2020b.

Liu, J., Liu, Z., Ma, Z., Yang, S., Yao, D., Zhao, S., Hu, B., Tang, G., Sun, J., Cheng, M., Xu, Z., and Wang, Y.: Detailed budget analysis of HONO in Beijing, China: Implication on atmosphere oxidation capacity in polluted megacity, Atmospheric Environment, 244, 10.1016/j.atmosenv.2020.117957, 2021.

Liu, Y., Han, C., Ma, J., Bao, X., and He, H.: Influence of relative humidity on heterogeneous kinetics of NO2 on kaolin and hematite, Phys Chem Chem Phys, 17, 19424-19431, 10.1039/c5cp02223a, 2015.

Liu, Y., Nie, W., Xu, Z., Wang, T., Wang, R., Li, Y., Wang, L., Chi, X., and Ding, A.: Semi-quantitative understanding of source contribution to nitrous acid (HONO) based on 1 year of continuous observation at the SORPES station in eastern China, Atmospheric Chemistry and Physics, 19, 13289-13308, 10.5194/acp-19-13289-2019, 2019b.

Liu, Y., Ni, S., Jiang, T., Xing, S., Zhang, Y., Bao, X., Feng, Z., Fan, X., Zhang, L., and Feng, H.: Influence of Chinese New Year overlapping COVID-19 lockdown on HONO sources in Shijiazhuang, Sci Total Environ, 745, 141025, 10.1016/j.scitotenv.2020.141025, 2020c.

Liu, Y., Lu, K., Li, X., Dong, H., Tan, Z., Wang, H., Zou, Q., Wu, Y., Zeng, L., Hu, M., Min, K. E., Kecorius, S., Wiedensohler, A., and Zhang, Y.: A Comprehensive Model Test of the HONO Sources Constrained to Field Measurements at Rural North China Plain, Environ Sci Technol, 53, 3517-3525, 10.1021/acs.est.8b06367, 2019c.

Liu, Y., Zhang, Y., Lian, C., Yan, C., Feng, Z., Zheng, F., Fan, X., Chen, Y., Wang, W., Chu, B., Wang, Y., Cai, J., Du, W., Daellenbach, K. R., Kangasluoma, J., Bianchi, F., Kujansuu, J., Petäjä, T., Wang, X., Hu, B., Wang, Y., Ge, M., He, H., and Kulmala, M.: The promotion effect of nitrous acid on aerosol formation in wintertime in Beijing: the possible contribution of traffic-related emissions, Atmospheric Chemistry and Physics, 20, 13023-13040, 10.5194/acp-20-13023-2020, 2020d.

Liu, Z., Wang, Y., Costabile, F., Amoroso, A., Zhao, C., Huey, L. G., Stickel, R., Liao, J., and Zhu, T.: Evidence

of aerosols as a media for rapid daytime HONO production over China, Environ Sci Technol, 48, 14386-14391, 10.1021/es504163z, 2014.

Lv, Z., Wang, X., Deng, F., Ying, Q., Archibald, A. T., Jones, R. L., Ding, Y., Cheng, Y., Fu, M., Liu, Y., Man, H., Xue, Z., He, K., Hao, J., and Liu, H.: Source-Receptor Relationship Revealed by the Halted Traffic and Aggravated Haze in Beijing during the COVID-19 Lockdown, Environ Sci Technol, 54, 15660-15670, 10.1021/acs.est.0c04941, 2020.

Ma, X., Tan, Z., Lu, K., Yang, X., Liu, Y., Li, S., Li, X., Chen, S., Novelli, A., Cho, C., Zeng, L., Wahner, A., and Zhang, Y.: Winter photochemistry in Beijing: Observation and model simulation of OH and HO2 radicals at an urban site, Sci Total Environ, 685, 85-95, 10.1016/j.scitotenv.2019.05.329, 2019.

Meng, F., Qin, M., Tang, K., Duan, J., Fang, W., Liang, S., Ye, K., Xie, P., Sun, Y., Xie, C., Ye, C., Fu, P., Liu, J., and Liu, W.: High-resolution vertical distribution and sources of HONO and NO2 in the nocturnal boundary layer in urban Beijing, China, Atmospheric Chemistry and Physics, 20, 5071-5092, 10.5194/acp-20-5071-2020, 2020.

Meusel, H., Tamm, A., Kuhn, U., Wu, D., Leifke, A. L., Fiedler, S., Ruckteschler, N., Yordanova, P., Lang-Yona, N., Pöhlker, M., Lelieveld, J., Hoffmann, T., Pöschl, U., Su, H., Weber, B., and Cheng, Y.: Emission of nitrous acid from soil and biological soil crusts represents an important source of HONO in the remote atmosphere in Cyprus, Atmospheric Chemistry and Physics, 18, 799-813, 10.5194/acp-18-799-2018, 2018.

Nie, W., Ding, A. J., Xie, Y. N., Xu, Z., Mao, H., Kerminen, V. M., Zheng, L. F., Qi, X. M., Huang, X., Yang, X. Q., Sun, J. N., Herrmann, E., Petäjä, T., Kulmala, M., and Fu, C. B.: Influence of biomass burning plumes on HONO chemistry in eastern China, Atmospheric Chemistry and Physics, 15, 1147-1159, 10.5194/acp-15-1147-2015, 2015.

Oswald, R., Behrendt, T., Ermel, M., Wu, D., Su, H., Cheng, Y., Breuninger, C., Moravek, A., Mougin, E., Delon, C., Loubet, B., Pommerening-Roser, A., Sorgel, M., Poschl, U., Hoffmann, T., Andreae, M. O., Meixner, F. X., and Trebs, I.: HONO emissions from soil bacteria as a major source of atmospheric reactive nitrogen, Science, 341, 1233-1235, 10.1126/science.1242266, 2013.

Peng, Q., Palm, B. B., Melander, K. E., Lee, B. H., Hall, S. R., Ullmann, K., Campos, T., Weinheimer, A. J., Apel, E. C., Hornbrook, R. S., Hills, A. J., Montzka, D. D., Flocke, F., Hu, L., Permar, W., Wielgasz, C., Lindaas, J., Pollack, I. B., Fischer, E. V., Bertram, T. H., and Thornton, J. A.: HONO Emissions from Western U.S. Wildfires Provide Dominant Radical Source in Fresh Wildfire Smoke, Environ Sci Technol, 54, 5954-5963, 10.1021/acs.est.0c00126, 2020.

Pusede, S. E., VandenBoer, T. C., Murphy, J. G., Markovic, M. Z., Young, C. J., Veres, P. R., Roberts, J. M., Washenfelder, R. A., Brown, S. S., Ren, X., Tsai, C., Stutz, J., Brune, W. H., Browne, E. C., Wooldridge, P. J., Graham, A. R., Weber, R., Goldstein, A. H., Dusanter, S., Griffith, S. M., Stevens, P. S., Lefer, B. L., and Cohen, R. C.: An Atmospheric Constraint on the NO2 Dependence of Daytime Near-Surface Nitrous Acid (HONO), Environ Sci Technol, 49, 12774-12781, 10.1021/acs.est.5b02511, 2015.

Qin, M., Xie, P., Su, H., Gu, J., Peng, F., Li, S., Zeng, L., Liu, J., Liu, W., and Zhang, Y.: An observational study of the HONO–NO2 coupling at an urban site in Guangzhou City, South China, Atmospheric Environment, 43, 5731-5742, 10.1016/j.atmosenv.2009.08.017, 2009.

R. Kurtenbach, K.H. Becker, J.A.G. Gomes, J. Kleffmann, J.C. L.orzer, M. Spittler, P. Wiesen, R. Ackermann, A. Geyer, and Platt, U.: Investigations of emissions and heterogeneous formation of HONO in a road traffic tunnel, Atmospheric Environment, , 3385–3394, 2001.

Rahmani, A., Khamutian, S., Doosti-Irani, A., Saatchi, O., and Shokoohizadeh, M. J.: Arsenic level in drinking water, its correlation with water quality parameters, and associated health risks, Environmental Monitoring and Assessment, 195, 10.1007/s10661-023-11486-1, 2023.

Shen, N., Zhao, X., Li, L., Zhou, B., Duan, F., and Zhao, W.: Spatial and temporal variation characteristics of

atmospheric NO2 and SO2 in the Beijing-Tianjin-Hebei region before and after the COVID-19 outbreak, Air Qual Atmos Health, 1-14, 10.1007/s11869-021-01016-8, 2021.

Song, M., Zhao, X., Liu, P., Mu, J., He, G., Zhang, C., Tong, S., Xue, C., Zhao, X., Ge, M., and Mu, Y.: Atmospheric NOx oxidation as major sources for nitrous acid (HONO), npj Climate and Atmospheric Science, 6, 10.1038/s41612-023-00357-8, 2023.

Song, Y., Zhang, Y., Xue, C., Liu, P., He, X., Li, X., and Mu, Y.: The seasonal variations and potential sources of nitrous acid (HONO) in the rural North China Plain, Environ Pollut, 311, 119967, 10.1016/j.envpol.2022.119967, 2022.

Spataro, F., Ianniello, A., Salvatori, R., Nardino, M., Esposito, G., and Montagnoli, M.: Sources of atmospheric nitrous acid (HONO) in the European High Arctic, Rendiconti Lincei, 28, 25-33, 10.1007/s12210-016-0568-9, 2016.

Stemmler, K.: Light induced conversion of nitrogen dioxide into nitrous acid on submicron humic acid aerosol, Atmospheric Chemistry and Physics, 2007.

Sun, J., Shen, Z., Zeng, Y., Niu, X., Wang, J., Cao, J., Gong, X., Xu, H., Wang, T., Liu, H., and Yang, L.: Characterization and cytotoxicity of PAHs in PM2.5 emitted from residential solid fuel burning in the Guanzhong Plain, China, Environ Pollut, 241, 359-368, 10.1016/j.envpol.2018.05.076, 2018.

Sun, J., Shen, Z., Cao, J., Zhang, L., Wu, T., Zhang, Q., Yin, X., Lei, Y., Huang, Y., Huang, R. J., Liu, S., Han, Y., Xu, H., Zheng, C., and Liu, P.: Particulate matters emitted from maize straw burning for winter heating in rural areas in Guanzhong Plain, China: Current emission and future reduction, Atmospheric Research, 184, 66-76, 10.1016/j.atmosres.2016.10.006, 2017.

Sun, Y., Lei, L., Zhou, W., Chen, C., He, Y., Sun, J., Li, Z., Xu, W., Wang, Q., Ji, D., Fu, P., Wang, Z., and Worsnop, D. R.: A chemical cocktail during the COVID-19 outbreak in Beijing, China: Insights from six-year aerosol particle composition measurements during the Chinese New Year holiday, Sci Total Environ, 742, 140739, 10.1016/j.scitotenv.2020.140739, 2020.

Sun, Y. L., Wang, Z. F., Fu, P. Q., Yang, T., Jiang, Q., Dong, H. B., Li, J., and Jia, J. J.: Aerosol composition, sources and processes during wintertime in Beijing, China, Atmospheric Chemistry and Physics, 13, 4577-4592, 10.5194/acp-13-4577-2013, 2013.

Tan, Z., Lu, K., Jiang, M., Su, R., Wang, H., Lou, S., Fu, Q., Zhai, C., Tan, Q., Yue, D., Chen, D., Wang, Z., Xie, S., Zeng, L., and Zhang, Y.: Daytime atmospheric oxidation capacity in four Chinese megacities during the photochemically polluted season: a case study based on box model simulation, Atmospheric Chemistry and Physics, 19, 3493-3513, 10.5194/acp-19-3493-2019, 2019.

Tan, Z., Hofzumahaus, A., Lu, K., Brown, S. S., Holland, F., Huey, L. G., Kiendler-Scharr, A., Li, X., Liu, X., Ma, N., Min, K. E., Rohrer, F., Shao, M., Wahner, A., Wang, Y., Wiedensohler, A., Wu, Y., Wu, Z., Zeng, L., Zhang, Y., and Fuchs, H.: No Evidence for a Significant Impact of Heterogeneous Chemistry on Radical Concentrations in the North China Plain in Summer 2014, Environ Sci Technol, 54, 5973-5979, 10.1021/acs.est.0c00525, 2020.

Tan, Z., Fuchs, H., Lu, K., Hofzumahaus, A., Bohn, B., Broch, S., Dong, H., Gomm, S., Häseler, R., He, L., Holland, F., Li, X., Liu, Y., Lu, S., Rohrer, F., Shao, M., Wang, B., Wang, M., Wu, Y., Zeng, L., Zhang, Y., Wahner, A., and Zhang, Y.: Radical chemistry at a rural site (Wangdu) in the North China Plain: observation and model calculations of OH, HO2 and RO2 radicals, Atmospheric Chemistry and Physics, 17, 663-690, 10.5194/acp-17-663-2017, 2017.

Tan, Z., Rohrer, F., Lu, K., Ma, X., Bohn, B., Broch, S., Dong, H., Fuchs, H., Gkatzelis, G. I., Hofzumahaus, A., Holland, F., Li, X., Liu, Y., Liu, Y., Novelli, A., Shao, M., Wang, H., Wu, Y., Zeng, L., Hu, M., Kiendler-Scharr, A., Wahner, A., and Zhang, Y.: Wintertime photochemistry in Beijing: observations of ROx radical concentrations in the North China Plain during the BEST-ONE campaign, Atmospheric Chemistry and Physics, 18, 12391-12411,

957 10.5194/acp-18-12391-2018, 2018.

958 Tang, M.-X., He, L.-Y., Xia, S.-Y., Jiang, Z., He, D.-Y., Guo, S., Hu, R.-Z., Zeng, H., and Huang, X.-F.: Coarse
959 particles compensate for missing daytime sources of nitrous acid and enhance atmospheric oxidation capacity in
960 a coastal atmosphere, Science of The Total Environment, 915, 10.1016/j.scitotenv.2024.170037, 2024.

961 Tong, S., Hou, S., Zhang, Y., Chu, B., Liu, Y., He, H., Zhao, P., and Ge, M.: Comparisons of measured nitrous
962 acid (HONO) concentrations in a pollution period at urban and suburban Beijing, in autumn of 2014, Science
963 China Chemistry, 58, 1393-1402, 10.1007/s11426-015-5454-2, 2015.

964 Tong, S., Hou, S., Zhang, Y., Chu, B., Liu, Y., He, H., Zhao, P., and Ge, M.: Exploring the nitrous acid (HONO)
965 formation mechanism in winter Beijing: direct emissions and heterogeneous production in urban and suburban
966 areas, Faraday Discuss, 189, 213-230, 10.1039/c5fd00163c, 2016.

967 VandenBoer, T. C., Young, C. J., Talukdar, R. K., Markovic, M. Z., Brown, S. S., Roberts, J. M., and Murphy, J.
968 G.: Nocturnal loss and daytime source of nitrous acid through reactive uptake and displacement, Nature
969 Geoscience, 8, 55-60, 10.1038/ngeo2298, 2014.

970 Wang, J., Xu, X., Wang, S., He, S., Li, X., and He, P.: Heterogeneous effects of COVID-19 lockdown measures
971 on air quality in Northern China, Appl Energy, 282, 116179, 10.1016/j.apenergy.2020.116179, 2021.

972 Wang, P., Chen, K., Zhu, S., Wang, P., and Zhang, H.: Severe air pollution events not avoided by reduced
973 anthropogenic activities during COVID-19 outbreak, Resour Conserv Recycl, 158, 104814,
974 10.1016/j.resconrec.2020.104814, 2020a.

975 Wang, S., Zhou, R., Zhao, H., Wang, Z., Chen, L., and Zhou, B.: Long-term observation of atmospheric nitrous
976 acid (HONO) and its implication to local NO2 levels in Shanghai, China, Atmospheric Environment, 77, 718-724,
977 10.1016/j.atmosenv.2013.05.071, 2013.

978 Wang, Y., Wen, Y., Wang, Y., Zhang, S., Zhang, K. M., Zheng, H., Xing, J., Wu, Y., and Hao, J.: Four-Month
979 Changes in Air Quality during and after the COVID-19 Lockdown in Six Megacities in China, Environmental
980 Science & Technology Letters, 7, 802-808, 10.1021/acs.estlett.0c00605, 2020b.

981 Weber, B., Wu, D., Tamm, A., Ruckteschler, N., Rodriguez-Caballero, E., Steinkamp, J., Meusel, H., Elbert, W.,
982 Behrendt, T., Sorgel, M., Cheng, Y., Crutzen, P. J., Su, H., and Poschl, U.: Biological soil crusts accelerate the
983 nitrogen cycle through large NO and HONO emissions in drylands, Proc Natl Acad Sci U S A, 112, 15384-15389,
984 10.1073/pnas.1515818112, 2015.

985 Wu, D., Horn, M. A., Behrendt, T., Muller, S., Li, J., Cole, J. A., Xie, B., Ju, X., Li, G., Ermel, M., Oswald, R.,
986 Frohlich-Nowoisky, J., Hoor, P., Hu, C., Liu, M., Andreae, M. O., Poschl, U., Cheng, Y., Su, H., Trebs, I., Weber,
987 B., and Sorgel, M.: Soil HONO emissions at high moisture content are driven by microbial nitrate reduction to
988 nitrite: tackling the HONO puzzle, ISME J, 13, 1688-1699, 10.1038/s41396-019-0379-y, 2019.

989 Xing, C., Xu, S., Song, Y., Liu, C., Liu, Y., Lu, K., Tan, W., Zhang, C., Hu, Q., Wang, S., Wu, H., and Lin, H.: A
990 new insight into the vertical differences in NO2 heterogeneous reaction to produce HONO over inland and
991 marginal seas, Atmospheric Chemistry and Physics, 23, 5815-5834, 10.5194/acp-23-5815-2023, 2023.

992 Xu, Z., Wang, T., Wu, J., Xue, L., Chan, J., Zha, Q., Zhou, S., Louie, P. K. K., and Luk, C. W. Y.: Nitrous acid
993 (HONO) in a polluted subtropical atmosphere: Seasonal variability, direct vehicle emissions and heterogeneous
994 production at ground surface, Atmospheric Environment, 106, 100-109, 10.1016/j.atmosenv.2015.01.061, 2015.

995 Xue, C.: Substantially Growing Interest in the Chemistry of Nitrous Acid (HONO) in China: Current
996 Achievements, Problems, and Future Directions, Environ Sci Technol, 10.1021/acs.est.2c02237, 2022.

997 Xue, C., Zhang, C., Ye, C., Liu, P., Catoire, V., Krysztofiak, G., Chen, H., Ren, Y., Zhao, X., Wang, J., Zhang, F.,
998 Zhang, C., Zhang, J., An, J., Wang, T., Chen, J., Kleffmann, J., Mellouki, A., and Mu, Y.: HONO Budget and Its
999 Role in Nitrate Formation in the Rural North China Plain, Environmental Science & Technology, 54, 11048-11057,
1000 10.1021/acs.est.0c01832, 2020.

Yang, D., Zhang, S., Niu, T., Wang, Y., Xu, H., Zhang, K. M., and Wu, Y.: High-resolution mapping of vehicle emissions of atmospheric pollutants based on large-scale, real-world traffic datasets, Atmospheric Chemistry and Physics, 19, 8831-8843, 10.5194/acp-19-8831-2019, 2019.

Yang, W., You, D., Li, C., Han, C., Tang, N., Yang, H., and Xue, X.: Photolysis of Nitroaromatic Compounds under Sunlight: A Possible Daytime Photochemical Source of Nitrous Acid?, Environmental Science & Technology Letters, 8, 747-752, 10.1021/acs.estlett.1c00614, 2021.

Ye, C., Gao, H., Zhang, N., and Zhou, X.: Photolysis of Nitric Acid and Nitrate on Natural and Artificial Surfaces, Environ Sci Technol, 50, 3530-3536, 10.1021/acs.est.5b05032, 2016.

Ye, C., Lu, K., Ma, X., Qiu, W., Li, S., Yang, X., Xue, C., Zhai, T., Liu, Y., Li, X., Li, Y., Wang, H., Tan, Z., Chen, X., Dong, H., Zeng, L., Hu, M., and Zhang, Y.: HONO chemistry at a suburban site during the EXPLORE-YRD campaign in 2018: formation mechanisms and impacts on O3 production, Atmospheric Chemistry and Physics, 23, 15455-15472, 10.5194/acp-23-15455-2023, 2023.

Yu, Y., Galle, B., Panday, A., Hodson, E., Prinn, R., and Wang, S.: Observations of high rates of NO2-HONO conversion in the nocturnal atmospheric boundary layer in Kathmandu, Nepal, Atmospheric Chemistry and Physics, 6401–6415, 2009.

Zhang, J., An, J., Qu, Y., Liu, X., and Chen, Y.: Impacts of potential HONO sources on the concentrations of oxidants and secondary organic aerosols in the Beijing-Tianjin-Hebei region of China, Sci Total Environ, 647, 836-852, 10.1016/j.scitotenv.2018.08.030, 2019a.

Zhang, J., Chen, J., Xue, C., Chen, H., Zhang, Q., Liu, X., Mu, Y., Guo, Y., Wang, D., Chen, Y., Li, J., Qu, Y., and An, J.: Impacts of six potential HONO sources on HOx budgets and SOA formation during a wintertime heavy haze period in the North China Plain, Sci Total Environ, 681, 110-123, 10.1016/j.scitotenv.2019.05.100, 2019b.

Zhang, J., Lian, C., Wang, W., Ge, M., Guo, Y., Ran, H., Zhang, Y., Zheng, F., Fan, X., Yan, C., Daellenbach, K. R., Liu, Y., Kulmala, M., and An, J.: Amplified role of potential HONO sources in O3 formation in North China Plain during autumn haze aggravating processes, Atmospheric Chemistry and Physics, 22, 3275-3302, 10.5194/acp-22-3275-2022, 2022a.

Zhang, L., Wang, T., Zhang, Q., Zheng, J., Xu, Z., and Lv, M.: Potential sources of nitrous acid (HONO) and their impacts on ozone: A WRF-Chem study in a polluted subtropical region, Journal of Geophysical Research: Atmospheres, 121, 3645-3662, 10.1002/2015jd024468, 2016.

Zhang, Q., Liu, P., George, C., Chen, T., Ren, Y., Mu, Y., Song, M., Herrmann, H., Mellouki, A., Chen, J., Zhao, X., and Zeng, Y.: Unveiling the underestimated direct emissions of nitrous acid (HONO), Proceedings of the National Academy of Sciences, 120, 10.1073/pnas, 2023a.

Zhang, W., Tong, S., Ge, M., An, J., Shi, Z., Hou, S., Xia, K., Qu, Y., Zhang, H., Chu, B., Sun, Y., and He, H.: Variations and sources of nitrous acid (HONO) during a severe pollution episode in Beijing in winter 2016, Sci Total Environ, 648, 253-262, 10.1016/j.scitotenv.2018.08.133, 2019c.

Zhang, W., Ren, Y., Zhang, C., Liu, P., Xue, C., Ye, C., Liu, C., Wang, J., Zhang, Y., Liu, J., Song, Y., Feng, Y., and Mu, Y.: Aging of pollution air parcels acts as the dominant source for nocturnal HONO, Sci Total Environ, 881, 163438, 10.1016/j.scitotenv.2023.163438, 2023b.

Zhang, W., Tong, S., Jia, C., Wang, L., Liu, B., Tang, G., Ji, D., Hu, B., Liu, Z., Li, W., Wang, Z., Liu, Y., Wang, Y., and Ge, M.: Different HONO Sources for Three Layers at the Urban Area of Beijing, Environ Sci Technol, 54, 12870-12880, 10.1021/acs.est.0c02146, 2020.

Zhang, X., Tong, S., Jia, C., Zhang, W., Wang, Z., Tang, G., Hu, B., Liu, Z., Wang, L., Zhao, P., Pan, Y., and Ge, M.: Elucidating HONO formation mechanism and its essential contribution to OH during haze events, npj Climate and Atmospheric Science, 6, 10.1038/s41612-023-00371-w, 2023c.

Zhang, X., Tong, S., Jia, C., Zhang, W., Li, J., Wang, W., Sun, Y., Wang, X., Wang, L., Ji, D., Wang, L., Zhao, P.,

1045 Tang, G., Xin, J., Li, A., and Ge, M.: The Levels and Sources of Nitrous Acid (HONO) in Winter of Beijing and
1046 Sanmenxia, Journal of Geophysical Research: Atmospheres, 127, 10.1029/2021jd036278, 2022b.

1047 Zhao, Y., Zhang, K., Xu, X., Shen, H., Zhu, X., Zhang, Y., Hu, Y., and Shen, G.: Substantial Changes in Nitrogen
1048 Dioxide and Ozone after Excluding Meteorological Impacts during the COVID-19 Outbreak in Mainland China,
1049 Environmental Science & Technology Letters, 7, 402-408, 10.1021/acs.estlett.0c00304, 2020.

1050 Zheng, B., Huo, H., Zhang, Q., Yao, Z. L., Wang, X. T., Yang, X. F., Liu, H., and He, K. B.: High-resolution
1051 mapping of vehicle emissions in China in 2008, Atmospheric Chemistry and Physics, 14, 9787-9805, 10.5194/acp-
1052 14-9787-2014, 2014.

1053 Zheng, J., Shi, X., Ma, Y., Ren, X., Jabbour, H., Diao, Y., Wang, W., Ge, Y., Zhang, Y., and Zhu, W.: Contribution
1054 of nitrous acid to the atmospheric oxidation capacity in an industrial zone in the Yangtze River Delta region of
1055 China, Atmospheric Chemistry and Physics, 20, 5457-5475, 10.5194/acp-20-5457-2020, 2020.

1056 Zhou, X., Zhang, N., TerAvest, M., Tang, D., Hou, J., Bertman, S., Alaghmand, M., Shepson, P. B., Carroll, M.
1057 A., Griffith, S., Dusanter, S., and Stevens, P. S.: Nitric acid photolysis on forest canopy surface as a source for
1058 tropospheric nitrous acid, Nature Geoscience, 4, 440-443, 10.1038/ngeo1164, 2011.

1059